International Journal of Fatigue 132 (2020) 105327

Contents lists available at ScienceDirect

International Journal of Fatigue

journal homepage: www.elsevier.com/locate/ijfatigue

Fatigue of offshore structures: A review of statistical fatigue damage assessment for stochastic loadings

Moises Jimenez-Martinez

Tecnologico de Monterrey, Escuela de Ingeniería y Ciencias, Via Atlixcáyotl 5718, Pue., Mexico

ARTICLE INFO

Keywords:
Offshore
Accelerated tests
Durability
Damage model
Spectrum

ABSTRACT

Structural offshore fatigue can be accelerated way to reduce the time required for testing. In this regard, a statistical analysis of the loads must be performed to reduce loads with low damage contribution, while the uncertainties from external sources are retained. This process generates the spectrum required to perform the accelerated tests. Subsequently, the spectrum can be extrapolated, which increases the damage and reduces the testing time. In this work, a review of the main types of offshore structures is presented, including a description of the main statistical signal process analysis. In addition, a review of the damage model used in offshore analysis is presented. This can be modelled as a Gaussian or narrow-band process, depending on the variable amplitude loading which generates a random process due to waves.

1. Introduction

Offshore infrastructure has extended its application from the oil and gas industry to the offshore wind industry. As a result of the increase in price and the fall in production, alternative sources of energy including renewable sources have been actively investigated. Many of these sources such as wave and wind are not new and have been used as energy sources for windmills and sailboats. However, changes have been made to these devices to obtain hydro-kinetic and hydro-potential energy from wave motion in order to exploit the worldwide wave power resource potential of 2 TW [1] using offshore energy structures such as ocean currents turbines, wave energy converters and both fixed and floating wind turbines. Offshore oil and gas extraction began at the end of the 19th century in the Caddo Lake in California with a wooden drilling platform. The stringent requirements to access production fields such as the Barent Sea and the Polar Seas suggest that there are regions that have not been fully exploited. This environment encourages companies to use stronger floating structures also known as platforms, that are used in the drilling and extraction process.

Pipelines are used to transport oil and gas from wellheads to the production facilities. Any failure during their service life is critical due to the associated physical and environmental risks. In 2016, over 2000 metric tons of oil and gas lack and spill. One of the most significant failure modes in offshore structures is due to fatigue [2,3] which occurs as a result of accumulated damage. As such, the structure can fail with loads below the yield strength [4]. Grouted connections for monopole foundations exhibit signs of a low capability for axial loads, which influences its durability test frequencies [5].

In addition to operational and loads from the wind, wave and current [6], the aggressive environment on offshore structures accelerate damage via corrosion, which is defined as metal wear that results from microbial reaction or by chemical or electrochemical attack. It can be monitored by several different methods including visual inspection of the component and its vicinity, evaluation of weight loss, the use of electrical resistance probes, and via acoustic emission testing. Its analysis is essential based on 15% of the leak and 21% of the failures in submarine gas pipelines is due to corrosion. The corrosion is not only external, internal corrosion also occurs due to the water content in oil and gas in addition to carbon dioxide, salts, organic acids and hydrogen sulphides [7].

Depending on the material strength fatigue process can be increased with the thickness and this effect is boosted with aggressive environment. This has to be evaluated carefully based on the saline environment, fatigue crack growth increase with decreasing frequency loads [8] the explanation is the aggressive damage exposure increase with low frequency. The analyse of corrosion fatigue effect, this has to be performed with testing, its important to evaluate and guarantee any failure on its structural components not only because offshore is a source of oil and gas also because offshore wind is an emerging sustainable energy source [9].

Some of the information presented in this report has been previously reviewed [10–13]. However, this work presents a detailed review of the statistical analysis and the damage evaluation result of stochastic loads from wind and wave generating random processes with

E-mail address: mjimenezm@tec.mx.

https://doi.org/10.1016/j.ijfatigue.2019.105327
Received 6 April 2019; Received in revised form 29 August 2019; Accepted 7 October 2019
Available online 14 October 2019

a focus on the offshore industry. In the next sections, the structures of the offshore oil and gas industry, as well as renewable sources are reviewed. The statistical processes for the time histories that are used to analyse the loads and their effect on the generation of the resulting spectrum to evaluate fatigue performance are considered. In the last section, the damage models used in the offshore industry are presented.

2. Offshore structures

Due to declining production from onshore wells, companies have been forced to identify new places to obtain oil and gas. In this regard, offshore sites have been investigated where drilling platforms are used to make wells in the sea bed. These can be used to explore and to extract oil from the well. In addition, production platforms are used after drilling and connect the sea bed with the sea surface via a production line. The fluid is handled using separation batteries and the oil and gas can be loaded or transferred using underwater pipelines. Depending on the capability of the platform, it is possible to pre-process or burn the gas.

The type of platform used depends on the depth of the water. In the case of shallow seas with a depth less than 100 m, platforms are built with a steel foundation on the sea bed with legs (Fig. 1a). For a depth between 200–300 m gravity platforms have been developed with foundations and legs made of concrete (Fig. 1b). A common type of platform using a framework or truss structure is capable of reaching a depth of 400 m (Fig. 1c). Since 1980, a variation of the truss platform has been implemented using mooring lines and is suitable for depths up to 800 m (Fig. 1d). For depths in the range of 800–1200 m, a floating platform without fixed connection with the sea bed is used. These platforms are known as tension leg platforms (Fig. 1e). For depths of 2000 m up to 3000 m, multi semi-submersible platforms are used. They are equipped with their own propulsion to avoid the effect of waves and increase overall stability (Fig. 1f). Finally, SPAR platforms are shaped as vertical cylinders as shown in Fig. 1g.

Renewable energy sources have been exploited to address the challenge of environmental pollution, however, there is still a significant reliance on fossil energy from gas and oil due to its resource limitations. Wind turbines can potentially be installed on offshore sites where the sea bed can be in the range of 40 m to >3000 m, where in addition to the depth, it is necessary to increase the number and size of wind turbines [14]. To achieve this, special structures have been used depending on the depth of the water Fig. 2. Monopiles are the most common foundation type [15], but these structures extend to a depth of only 30 m. Another type is a Jacket or Tripod support structures. For depths from 50 to 120 m, floating structures (Tension and Semi-submersibles) are used. Spar floating structures are used for depths above 120 m. For these structures, the loads are attributed to the basis and the wind [2].

2.1. Risers

The offshore oil and gas industry often operate in deep water below 3000 m, thereby exposing mechanical components such as pipelines, umbilicals and risers to low temperatures and high external pressures. Failures in these components are primarily attributable to mechanical damage, external or internal corrosion and fatigue [16]. An important component is the riser, which transfers oil and gas (Fig. 3). Failure of this structure does not only affect its operation, the may environment may also be affected. To reduce the risk of failure, conservative designs are implemented with safety factors for steel catenary risers between 7 and 10 [17]. For temporary systems, a fatigue design factor of 3 is used [18]. In the case of shearing loads due to bending to generate freeting, a safety factor of 10 is defined [19].

Pipelines can be deformed circumferentially and axially as a result of the fluid flow temperature, buckling and overbending, resulting in longitudinal compressive stress. Fig. 3 shows an internal section of a riser.

Failure in risers is different depending on their kind. In flexible risers, the common failures are due to fatigue corrosion, torsion, bursting, collapse and overbending. In the case of rigid risers, failure is due to impact, overstress, fatigue, structural wear, structural instability, material wear, external corrosion for protection failure or internal corrosion. Umbilical cables are significantly affected during riser installation. Moreover, the generation of residual stresses is the main cause of their failure due to tension or compression, torsion and fatigue [16]. Fig. 4 shows several different geometries of risers.

Corrosion fatigue is the result of the combined effect of mechanical stress and stress corrosion for materials such as aluminium and titanium alloys, as well as steel. It is dependent on the frequency and the waveform of the load [20].

Corrosion increases crack growth. To extend the fatigue life, it is necessary to minimize corrosion. This phenomenon can be controlled by tailoring the corrosivity of the environment and modifying the pipeline material with alloying elements, coatings, cathodic protection,

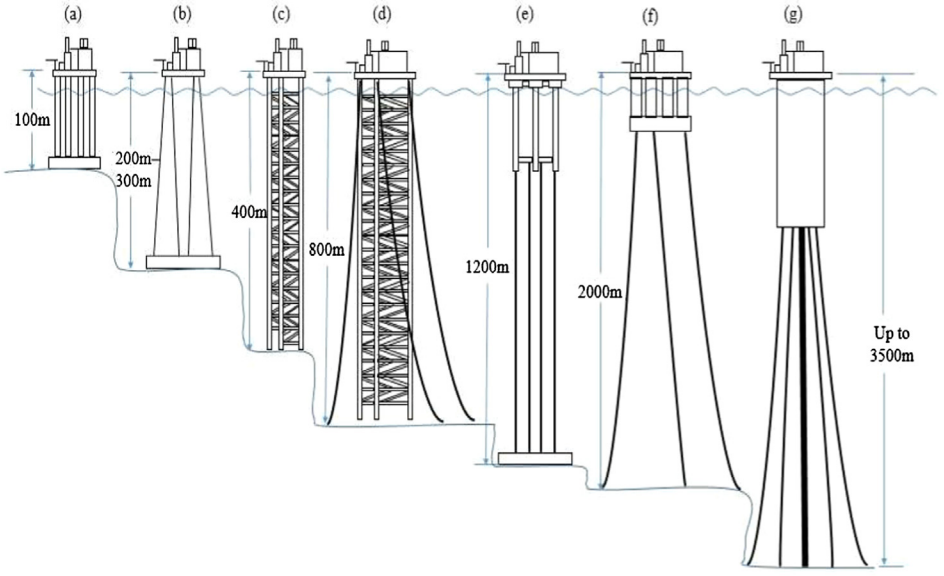

Fig. 1. Oil and gas platforms.

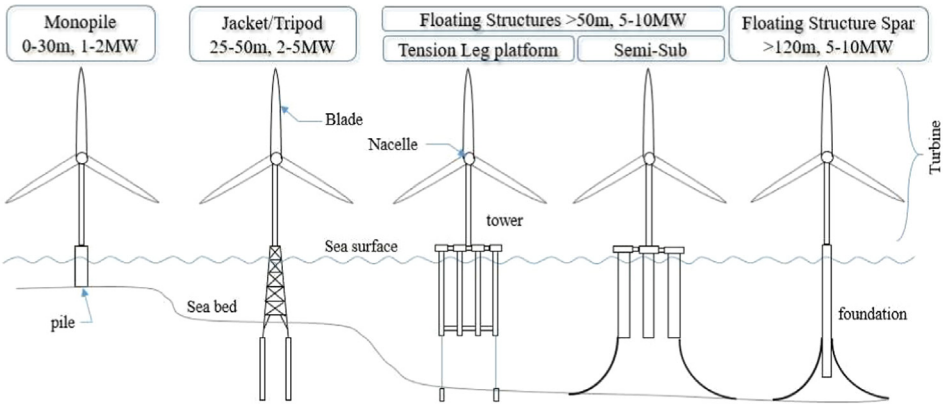

Fig. 2. Offshore wind support structures (adapted from [9]).

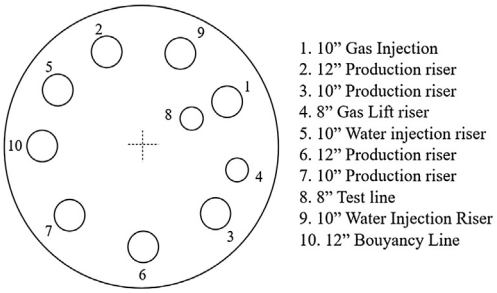

Fig. 3. Internal structure of riser.

linings, and metal cladding. Pipeline material with low chromium content is affected by corrosion due to the presence of chloride, hydrogen sulphide and CO2. To address the issue of fatigue damage, carbon manganese steel is used [7].

Corrosion reduces the strength of the pipeline. During normal operation, pressure build up can result in bursts or leakage. Leakage occurs when the corrosion penetrates the thickness of the pipelines, while burst occurs when the operating pressure exceeds the maximum allowable pressure at a weak point. During ultra-deep operations, a reduction in thickness can cause a collapse under the influence of the high external pressure instead of burst under high internal pressure. Most leaks due to internal corrosion can be explained by microbiologically induced corrosion (MIC) or by ingress of CO2 traces combined with H2S. The corrosion pattern is in the form of pits, craters, or uniform wall thinning.

Considering all failures, fatigue is the most common because it is associated with the wear of the armour corrosion fatigue polymeric [16]. There is a significant stiffness effect between the riser and the connector near the end. To minimize the corrosion effect in subsea equipment, cathodic protection is used for external surfaces. For workover riser and wellhead systems, sacrificial anodes are used. In the case of joints, a metal coating is applied [18].

Another kind of load generating structural damage in risers is vortex-induced vibration (VIV). [21] proposed a response reconstruction based on a spatial Fourier decomposition in terms of sine and cosine terms. Damage is evaluated using the Rainflow method via an S-N curve where the total stress is the sum of the stress of the main harmonics.

An external source of loads originates from waves and ocean currents [7]. There is a relationship between wave height and fatigue [2]. There is a relationship between wave height and fatigue. For fatigue,

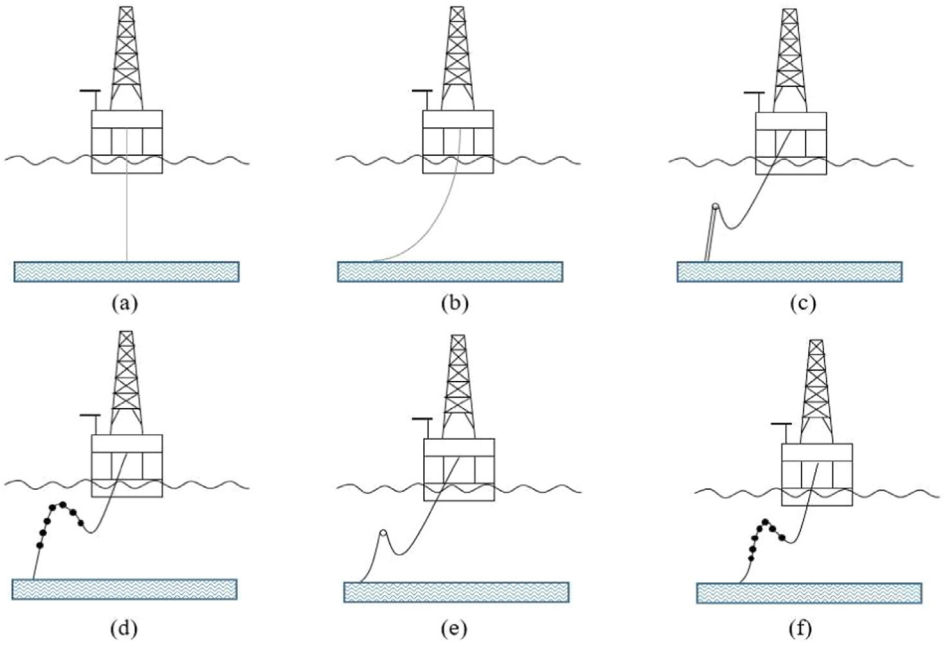

Fig. 4. Riser geometries (a) Rigid, (b) Simple catenary, (c) Steep-s, (d) Steep-wave, (e) Lazy-s and (f) Lazy wave.

life prediction is important to obtain reliable wave statistics and a stochastic description of sea state during service life. Wave statistics are provided in a wave scatter diagram to get the joint probability of wave height and mean wave period [22]. Cerveira et al. [23] used a wave scatter diagram of the Portuguese Pilot zone to analyze the mooring system effects on the dynamics of a floating wave energy converter. Videiro et al. [24] presented the Key Region Long-Term Analysis (KRLTA) method to estimate long-term responses of offshore structures by wave loads based on the response surfaces over the wave heights and periods with effective contribution in the scatter diagram. Ma et al. [25] proposed an improved mixture simulation that expanded the wind-wave scatter from the wave scatter diagram to include the average wind speed of the fluctuating wind.

The basis for the fatigue damage approach is to compare the loads on the component generated during its function, with the material properties using a damage rule. Depending on the time history, this can be directly applied to the number of repetitions for constant amplitude loads or if necessary, to the analysis of the spectrum generated by the time history, as described by Jimenez 2017 [12].

The Van der Pol wake oscillator model can be used to modulate the fatigue life for the vortex induced vibration. The parameters can be related to the riser variables and the force depends on the structure's acceleration. The excitation of the structure's acceleration can be modelled as:

$$\frac{\partial^2 y}{\partial t^2} + \frac{\gamma\omega_f}{\mu}\frac{\partial y}{\partial t} - c^2\frac{\partial^2 y}{\partial z^2} + b^2\frac{\partial^4 y}{\partial z^4} = \omega_f^2 Mq,$$
$$\frac{\partial^2 q}{\partial t^2} + \varepsilon\omega_f(q^2-1)\frac{\partial q}{\partial t} + \omega_f^2 q = A\frac{\partial^2 y}{\partial t^2}, \tag{1}$$

where $\gamma = CD/(4\pi St)$ is the stall coefficient, $\omega_f = \Omega_{Ref(z)}/\Omega_{Ref} = U_{Ref(z)}/U_{Ref}$ is the nondimensional shedding frequency, $\mu = (m_c yl + m_f luid)/\rho D^2$ is the mass ratio, $c^2 = [K/(m_{cyl} + m_{fluid}]/(\Omega_{Ref}R)^2$ is the nondimensional tension, $b^2 = [K/(m_{cyl} + m_{fluid})]/(\Omega_{Ref}D)^2$ is the nondimensional bending stiffness, $M = C_{LO}/(28\pi^2 St^2\mu)$ is a coefficient of the forcing term that acts on the structure due to the wake dynamics, and A and ϵ are the Van der Pol's coefficients.

Munkadan [26], proposed a change in this model based on a fluctuation life coefficient (C_{LO}) and drag coefficient (C_O) as the random parameters

$$\varepsilon(\zeta) = \varepsilon_m\left[1 + \sigma_\zeta\left(\xi_\zeta + \sum_{i=1}^{N} g_j(\zeta,\xi)\right)\right],$$
$$A(\zeta) = A_m\left[1 + \sigma_\zeta\left(\xi_\zeta + \sum_{i=1}^{N} g_j(\zeta,\xi)\right)\right], \tag{2}$$

$$C_L(\zeta) = C_{LOm}\left[1 + \sigma_\zeta\left(\xi_\zeta + \sum_{i=1}^{N} g_j(\zeta,\xi)\right)\right],$$
$$C_D(\zeta) = C_{Dm}\left[1 + \sigma_\zeta\left(\xi_\zeta + \sum_{i=1}^{N} g_j(\zeta,\xi)\right)\right], \tag{3}$$

where $\zeta = z/L$, z is the position along the length of the riser, ξ is a random number, σ_ζ is the standard deviation and g is a continuous function with a random peak along the length.

The analyses of marine risers can be modelled as beams and the most common is the nonlinear Euler-Bernoulli that takes variable loads into consideration. It is important to analyse this phenomenon because the internal resonances can increase the amplitudes, thereby accelerating damage [2]. Based on its assembly characteristic, an inclination is common and it is fixed at both ends to connect the sea surface to the sea bed. It can be expressed as follows:

$$m\frac{\partial^2\hat{y}_t}{\partial_{\hat{t}}{}^2} + EI\frac{\partial^4\hat{y}_t}{\partial_{\hat{t}}{}^4} - \left(T_e - We sin(\theta)(L-\hat{x}) + \frac{EA_p}{2L}\int_0^L\left(\frac{\partial\hat{y}_t}{\partial\hat{x}}\right)^2 d\hat{x}\right)\left(\frac{\partial^2\hat{y}_t}{\partial_{\hat{x}}{}^2}\right) - W_e sin(\theta)\left(\frac{\partial\hat{y}_t}{\partial\hat{x}}\right) + \bar{c}\frac{\partial\hat{y}_t}{\partial\hat{t}} = F_d - W_e cos(\theta). \tag{4}$$

Based on the next boundary conditions, i.e.,

$$\hat{y}_t(\hat{x},\hat{t}) = 0. \tag{5}$$

with $\hat{x} = 00$ and $\hat{x} = LL$, where $\hat{y}_t$t is the deflection of the riser along the position $\hat{y}_t$ and time $\hat{t}$, mm is the total mass per unit length including the mass per unit length ma and the mass of the riser pipe mp, EI is the flexural rigidity, W_e is the apparent weight of the riser per unit length modelled as $W_e = (mp - \rho_e A_e)g$, ρ_e is the density of the seawater, A_e is the area based on the outside diameter of the riser pipe, T_e is the applied tension, θ is the inclination angle, L is the length of the pipe, A_p is the cross section area of the pipe, $\bar{c}$ is the damping coefficient and F_d is the external dynamic forces. The load conditions depend on the operational conditions and the structural assembly.

3. Fatigue evaluation

It is important to evaluate components using experimental tests because fatigue strength has inherent scattering due to four main parameters: the loading, design, manufacturing and material [12]. These factors modify the SN curves in addition to the environment if is in air or in seawater with cathodic protection [18]. The most widely used life prediction is based on a comparison of the applied loads with the component's material fatigue strength. The most precise information is measured in this regard. The load in service are acquired analysed as is shown in Fig. 5, in offshore and the waves develop a nonlinear structural behaviour [6]. Another approach is to evaluate the damage. Instead of recording the signal for analysis and postprocessing, the acquired signal is used for continuous monitoring to evaluate the structural performance based on the assumption that the damage changes the mass and structural stiffness [14].

The monitoring is performed with instrumentation to measure variables that can generate stress on the component. This variable is measured to evaluate its response. In order to generate a record of the loads, different conditions are considered during the period of measurement. It is necessary to include the most relevant operational conditions such as when the well is flowing at a different rate to include the presence of gas bubbles that generate internal turbulence. Or in the case of wind structures, when the turbine is rotating at its maximum velocity thereby stressing the nacelle supports and generating the major loads of the tower and foundation.

The result of the acquisition is a time history as shown in Fig. 6. Based on the load history, the analysis can be performed in the time or frequency domain [27]. The time domain considers the nonlinearities of the system and the excitations. However, high accuracy is necessary for offshore to measure a long-term wave condition to obtain the stochastic uncertainties [4].

The spectrum of time histories for constant amplitude is linear, for variable amplitude is a curve generated by the cycle counting. Stochastic loads can be modelled with stationary Gaussian process to estimate the expected damage from the Power Spectrum density [28]. The synthesized signal can be reproduced or can be used standardized load spectra [29,12].

The spectrum of the time history for constant amplitude is linear. For a variable amplitude, it is a curve generated by cycle counting. Stochastic loads can be modelled according to a stationary Gaussian process to estimate the expected damage from the density of the power spectrum [28]. The synthesized signal can be reproduced or can be used as the standardized load spectra [29,12].

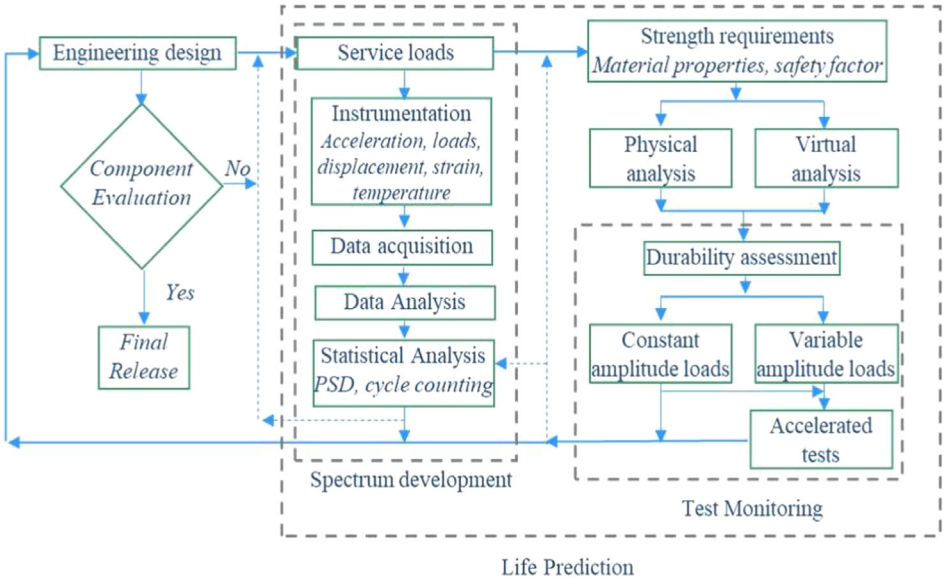

Fig. 5. Parameters influencing the structural durability of components.

3.1. Statistical analysis

The time history must be analysed to understand the physical behaviour of the structure. Fig. 7 shows a schematic waveform. The main characteristic is the nominal stress amplitude S_a. If it has a constant amplitude, the stress range S_R is constant and is defined by the difference between the maximum stress (S_{max}) and minimum (S_{min}) in a cycle, i.e.:

$$S_R = S_{max} - S_{min}. \tag{6}$$

$$S_a = \frac{S_R}{2} = \frac{S_{max} - S_{min}}{2}. \tag{7}$$

The mean stress S_m is defined as:

$$S_m = \frac{S_{max} + S_{min}}{2}. \tag{8}$$

A fully alternating stress $S_m = S_a$

The stress ratio R is defined as the ratio of the minimum to maximum stress as follows:

$$R = \frac{S_{min}}{S_{max}}. \tag{9}$$

The fatigue damage of a component is influenced by the mean stress expressed by its stress ratio in the high cycle region. Under normal circumstances $R \geqslant 0$, its propagation is accelerated by open microcracks while for $R = \infty$ or >1, the microcrack closes, which is beneficial for fatigue strength. In the low cycle region, plastic deformation

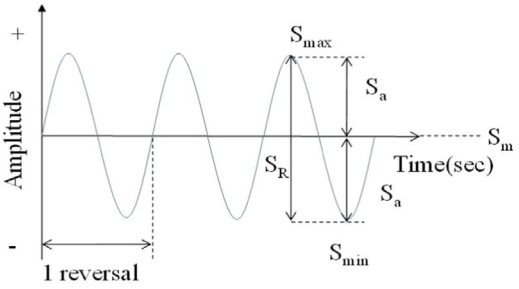

Fig. 7. Signal characteristics.

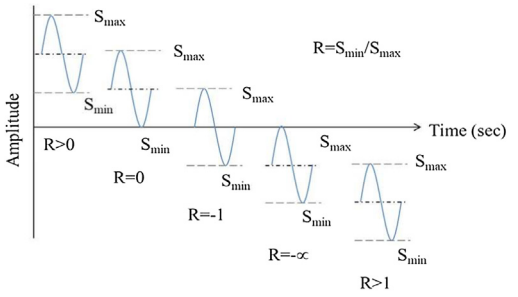

Fig. 8. Stress ratio.

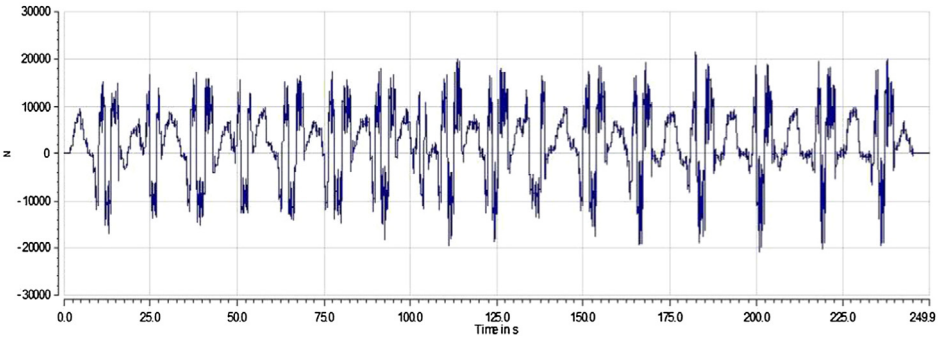

Fig. 6. Load time history.

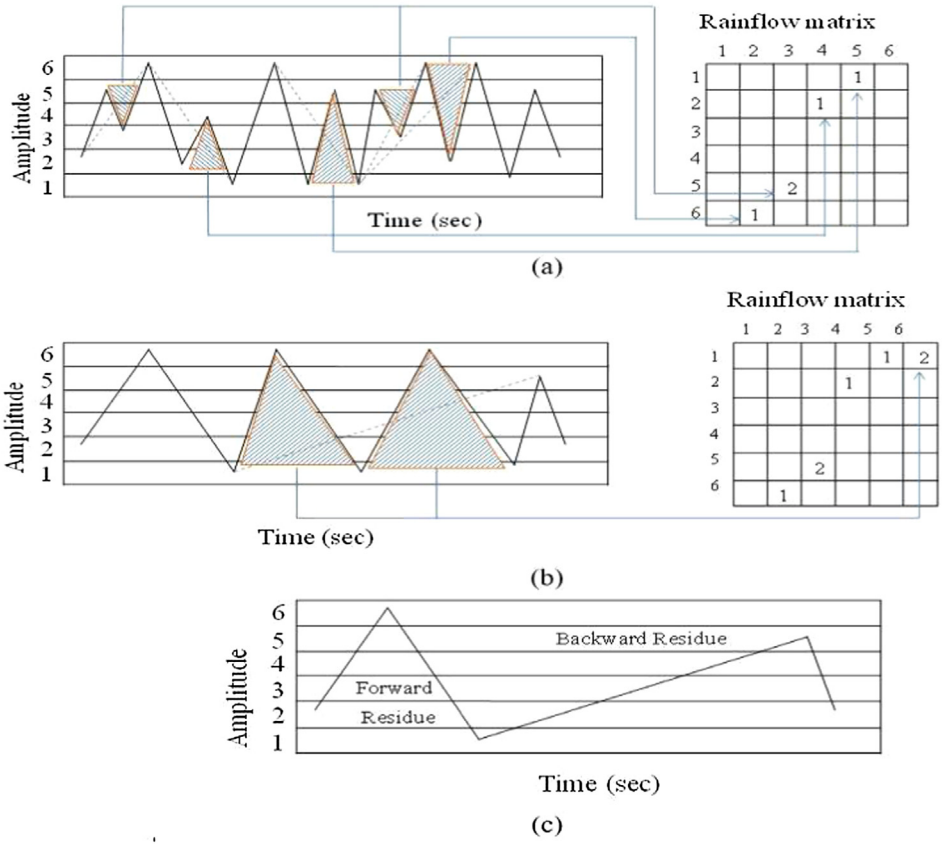

Fig. 9. Rainflow counting process (a) initial counting, (b) continued counting and (c) residue.

eliminates the effect of mean stress to improve or reduce the fatigue strength. The schematic stress ratio per cycle is shown in Fig. 8.

The amplitude ratio is the ratio of the stress amplitude to mean stress.

$$A = \frac{a}{m} = \frac{1-R}{1+R}. \tag{10}$$

The loads are monitored using cycle counting which is used to summarize the variable amplitude time histories and facilitates the repetitions of the load during the time history [12]. There are different cycle counting methods such as the Rainflow used to extract cycles from random histories in the time domain [30,10]. This approach is based on the analogy of raindrops falling on a roof. This is the best method to estimate fatigue damage [27] and it is widely used to process random Signals [31]. Fig. 9 shows the Rainflow counting process.

The cycle counting is represented in a matrix as shown in Fig. 9. The signals have 2 cycles from 5 to 3, 1 cycle from 6 to 3, 1 cycle from 1 to 5, 1 cycle from 2 to 4 (Fig. 9a), 2 cycles from 1 to 6 (Fig. 9b) and it has a reside as shown in Fig. 9c. These cycles are tabulated in a matrix which can be represented by a colour depending on the counts.

There is one parameter cycle counting method to extract the number of reversals in a variable amplitude time history. For the range pair shown in Fig. 10, the magnitude of the loads is split into several levels and the result is tabulated in Fig. 10b. Table 1 summarizes the counting events in Fig. 10.

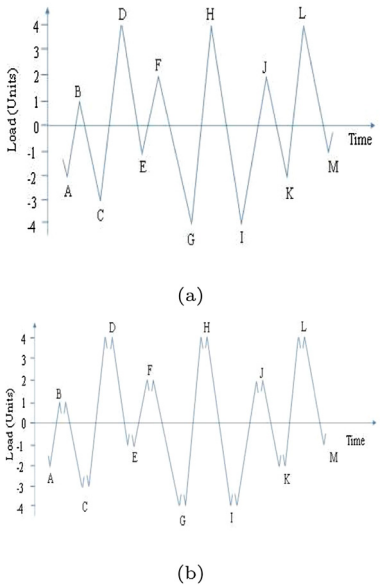

Fig. 10. Range pair counting process (a) time signal and (b) events.

3.2. Level crossing rate of narrow-band random process

For a stationary process $X(t)$ continuous and differentiable the counting of positive slopes crossing, infinitesimal intervals only depend on the increment of time d_t and the upcrossing expected rate is $(\upsilon a +)$ as:

For a stationary process $X(t)$ that is continuous and differentiable, for the counting of positive slope crossing, the infinitesimal intervals only depend on the increment of the time dt and the up-crossing expected rate is $(\upsilon a +)$:

$$E[N_a + (dt)] = \upsilon_a + dt. \tag{11}$$

If A is an event that a random sample from the stationary process $X(t)$ has a positive sloped crossing $x = a$ in dt, its probability $P(A)$ is

If A is the event that a random sample from the stationary process $X(t)$ has a positive-sloped crossing $x = a$ in dt, then its probability $P(A)$

Table 1
Range pair counting.

Range (Units)	*Cycle counts*	*Events*
8	1.0	$G-H, H-I$
7	0.5	$C-D$
6	1.5	$F-G, I-J, K-L$
5	1.0	$D-E, L-M$
4	1.0	$B-C, J-K$
3	1.0	$A-B, E-F$
2	0.0	
1	0.0	

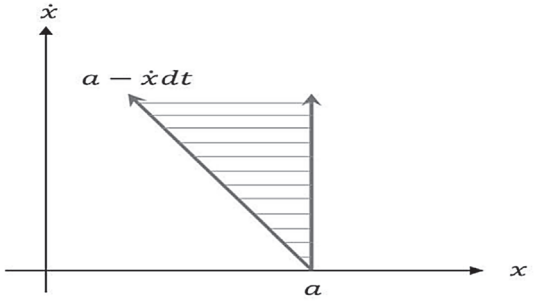

Fig. 11. Region for an event in the $x(t)-\dot{x}(t)$ plane.

is given by:

$$P(A) = \upsilon_a + dt. \tag{12}$$

for the following conditions $a - x(t) < x(t) < a$ and $\dot{x}(t) > 0$.

Based on these conditions $P(A)$ defines a triangular area (Fig. 11) and can be rewritten as follows:

$$P(A) = P(a - x(t)) < x(t) < a \cap \dot{x}(t) > 0 \tag{13}$$

To compute the probability of A, we integrate the probability density function (PDF):

$$P(A) = \int_0^{\infty} \int_{a-vdt}^{a} fx\dot{x}(u, v)dudv \tag{14}$$

Substituting (13) into (11), the up-crossing rate is:

$$\upsilon_{a+} = \int_0^{\infty} vfx\dot{x}(a, v)dv \tag{15}$$

For a Gaussian $X(t)$ the expected up-crossing rate can be expressed as follows:

$$\upsilon_{a+} = \frac{1}{2\pi}\frac{\sigma\dot{x}}{\sigma x}exp\left(\frac{-a^2}{2\sigma^2}\right) \tag{16}$$

If a = 0, the expected rate $E[0^+]$ is (Eq. (17)):

$$E[0^+] = \frac{1}{2\pi}\frac{\sigma\dot{x}}{\sigma x} = \sqrt{\frac{\int_0^{\infty} f^4 W_x(f)df}{\int_0^{\infty} f^2 W_x(f)df}} \tag{17}$$

The velocity rate of zero down crossing occurs of a peak in $\dot{x}(t)$ and for a Gaussian process is shown in Eq. (17): The velocity rate of zero down-crossing occurs at a peak in $\dot{x}(t)$) and for a Gaussian process, it is represented by Eq. (18):

$$E[P] = \frac{1}{2\pi}\frac{\sigma\dot{x}}{\sigma x} = \sqrt{\frac{\int_0^{\infty} f^4 W_x(f)df}{\int_0^{\infty} f^2 W_x(f)df}} \tag{18}$$

In a narrow band process for every peak there is a corresponding zero upcrossing. For a wide band process is not smooth and harmonic as narrow, to analyze it's a irregularity factor (γ) is used to define this ratio as shown in Eq. (19), this is a measure of the fluctuation of the load with its mean load, an example is shown in Fig. 12.

In a narrow-band process, for every peak, there is a corresponding zero up-crossing. A wide-band process is not smooth and the harmonics as narrow. In the analysis process, its irregularity factor (γ) is used to define this ratio as defined in Eq. (19). This is a measure of the fluctuation of the load with its mean load. An example is shown in Fig. 12.

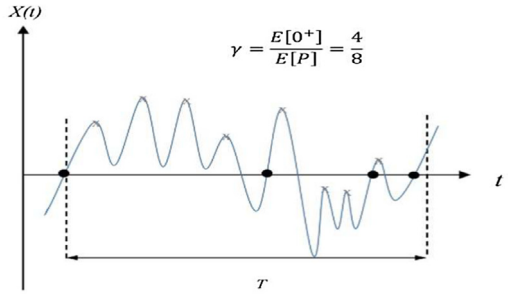

Fig. 12. Irregularity factor.

$$\gamma = \frac{number\ of\ mean\ value\ crossings}{number\ of\ extrema} = \frac{E[0^+]}{E[P]} \tag{19}$$

When $\gamma \to 0$ there is a tendency to more peaks for every zero up-crossing and represents wide band random process. When $\gamma = 1$ is to a peak per zero upcrossing to get a narrow band process. Another way to define the type of process is based on the spectral width parameter λ , that is expressed in Eq. (20):

When $\gamma \to 0$, there is a tendency for more peaks to be generated for every zero up-crossing and this represents the wide-band random process. When $\gamma = 1$, there is a peak per zero up-crossing to achieve a narrow-band process. Another way to define the type of process is based on the spectral width parameter λ which is expressed in Eq. (20):

$$\lambda = \sqrt{1-\gamma^2}, \tag{20}$$

where $\lambda \to 0$ is a narrow band random process.

Fig. 13 shows the moments from a one-sided PSD. If M_j is the $j_t h$ moment, the zero crossing and peak rates are defined as shown in Eq. (21).

$$M_j = \int_0^{\infty} f^j WS_a(f)df. \tag{21}$$

The parameters from the moments are:

$$E[0^+] = \sqrt{\frac{M_2}{M_0}}, \tag{22}$$

$$E[P] = \sqrt{\frac{M_4}{M_2}}, \tag{23}$$

The irregularity factor (γ) of the signal is:

$$\gamma = \sqrt{\frac{M_2^2}{M_0 M_4}}, \tag{24}$$

and the spectral width parameter, (λ) , becomes:

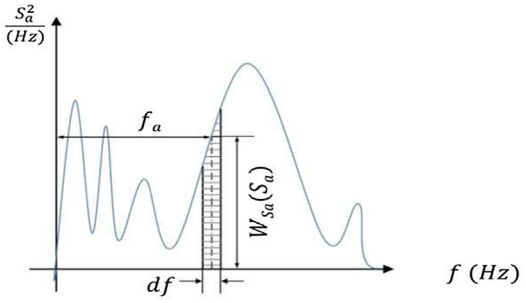

Fig. 13. Moments for one-side PSD.

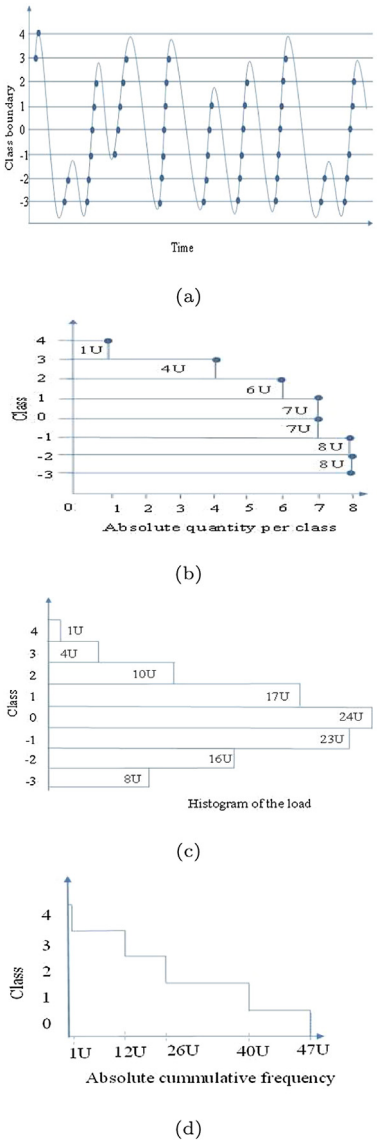

Fig. 14. Level crossing counting process (a) time history, (b) quantity per class, (c) histogram and (d) absolute cumulative frequency.

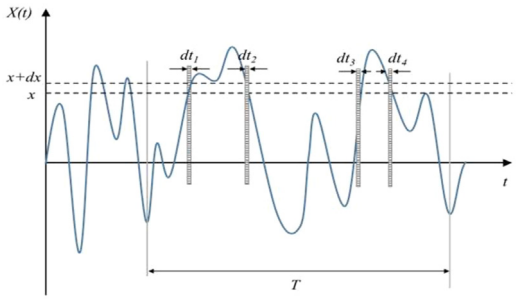

Fig. 15. Probability density function (PDF) for a random process X(t).

$$\lambda = \sqrt{1 - \frac{M_2^2}{M_0 M_4}}, \tag{25}$$

The amplitudes of the loads are split into several levels based on the range. The load is counted when it has a peak at different levels, which causes a change of its slope from positive to negative or negative to positive. The cycle counting is shown in Fig. 14 (see Fig. 15)

The *PSD* for dynamic analysis is widely used in offshore field [13]. The advantage to analyze the responses with *PSD* is due to it represents the energy of the time signal at each frequency. Fast Fourier Transform (*FFT*) can be used to obtain the *PSD* of the amplitude time history, where its inverse could be used to build the signal in time domain. For a time history with an excitation or motion response $X(t)$ its probability density function (PDF) is obtained based on its statistical properties. For a variable amplitude load where is extracted an amplitude as a function of the time $x(t)$ in the interval T, the function is found in the range x and $x + dx$, defining the probability $f_x(x)$ in this range is expressed in Eqs. (26) and (27).

The *PSD* for dynamic analysis is widely used in the offshore field [13]. It is advantageous to analyze the responses using *PSD* because it represents the energy of the time signal at each frequency. The Fast Fourier Transform (*FFT*) can be used to obtain the *PSD* of the amplitude-time history and its inverse could be used to build the signal in the time domain. For a time-history with an excitation or motion response $X(t)$, its probability density function (*PDF*) can be obtained based on its statistical properties. For a variable amplitude load whereby the amplitude is determined as a function of time $x(t)$ in the interval T, the function is in the range x and $x + dx$. The probability $f_x(x)$ in this range can be expressed as:

$$P[x \leqslant X(t) \leqslant x + dt] = \frac{dt_1 + dt_2 + dt_3 + dt_4}{T}, \tag{26}$$

$$f_x(x) = P[x \leqslant X(t) \leqslant x + dt] = \frac{\sum_{i=1}^{k} dt_i}{T}, \tag{27}$$

The *PDF* can also be obtained by using the fraction of the total number of samples by digitizing the signal with a sampling rate as is shown in Fig. 16, where $f_x(x)$ is given by Eq. (28).

$$f_x(x) = P[x \leqslant X(t) \leqslant x + dt] = \frac{\#sample_{band}}{\#sample_T}. \tag{28}$$

For a given probability density function, the mean (μ_x) and the variance (σ_x^2) are expressed by Eq. (29) and (30) respectively, as follows:

$$\mu_x = \int_{-\infty}^{+\infty} x f_x(x) dx \cong \frac{1}{T} \int_0^T X(t) dt, \tag{29}$$

$$\sigma_x^2 = \int_{-\infty}^{+\infty} [x - \mu x]^2 f_x(x) dx \cong \frac{1}{T} \int_0^T [X(t) - \mu_x]^2 dt. \tag{30}$$

When the mean of the process (μ_x) = 0, the standard deviation σ_x is the root mean square of $X(t)$, this value is a measure of the amplitude. If the process follows a bell-shaped distribution, the *PDF* is given according to Eq. (31):

$$f_x(x) = \frac{1}{\sqrt{2\pi}\sigma_x} exp\left[-\frac{1}{2}\left(\frac{x - \mu_x}{\sigma_x}\right)^2\right] \tag{31}$$

Time histories can be split into constant amplitude or variable amplitude. The last one is the most common based on the random process of the loads, this series of points $x1(t)$, $x2(t)$, ...,$xn(t)$ build the history $x(t)$.

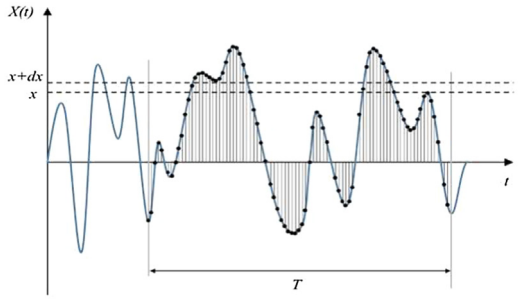

Fig. 16. Probability density function for a digitized random process X(t).

Time histories can be split into constant amplitude or variable amplitude with the latter being the most common. Based on the random process of the loads, the series of points $x1(t)$, $x2(t)$, ...,$xn(t)$ builds the history $x(t)$.

This ensemble makes a random process such that the probability density depends on the process. This is stationary if the probability distributions remain stationary, which implies that its statistical properties such as the mean standard deviation and the mean square are time-invariant. If these properties are the same along any sample as across the ensemble, the process is called ergodic. An ergodic process must be stationary, but a stationary process is not necessarily ergodic.

The autocorrelation function $E[x(t1)x(t2)]$ of a random process is the mean value of the product $x(t1)x(t2)$ and approximated is the average value. For a stationary random process this is time invariant and depends only on the time difference $\tau = |t_2 - t_1|$ getting that the autocorrelation function of $X(t)$ is a function of τ and can be expressed by $R(_\tau)$ as follows (Eq. (32)):

The autocorrelation function $E[x(t1)x(t2)]$ of a random process is the mean value of the product $x(t1)x(t2)$ and is approximated by the average value. For a stationary random process, this is time-invariant and depends only on the time difference $\tau = |t_2 - t_1|$, indicating that the autocorrelation function of $X(t)$ is a function of τ and can be expressed by $R(_\tau)$ as follows (Eq. (32)):

$$R(\tau) = E[X(t_1)X(t_2)]. \tag{32}$$

The associated mean (μ_x) and standard deviation (σ_x) are independent of the correlation coefficient (ρ). For $x(t_1)$ and $x(t_2)$, they are given by:

$$E[x(t_1)] = E[x(t_2)] = \mu_x \tag{33}$$

$$\sigma_{x(t_1)} = \sigma_{x(t_2)} = \sigma_x \tag{34}$$

$$\rho = \frac{R_x(\tau) - \mu_x^2}{\sigma_x^2} \tag{35}$$

The values of ρ are between -1 and 1 obtaining a low correlation when its value are near of 0 and best correlation when reach 1. This is expressed in Fig. 17 and Eq. (35) (see Fig. 18).

The values of ρ are between -1 and 1. A low correlation is obtained when it has a value near 0 and the best correlation is obtained when the value is 1. This is expressed in Fig. 17 and Eq. (35).

$$\mu_x^2 - \sigma_x^2 \leqslant R_x\tau \leqslant \mu_x^2 + \sigma_x^2. \tag{36}$$

When the time interval approaches infinity, the random variables $x(t_1)$ and $x(t_2)$ are not correlated and ρ tends to 0. For a time interval of 0, we have:

$$R_x(\tau = 0) = \mu_x^2 + \sigma_x^2 = E[X^2]. \tag{37}$$

$$R_x(0) = E[X^2], \tag{38}$$

A periodic time history $X(t)$ can be built using the summation of sinusoidal waves. For a period T, $X(w)$ is the forward Fourier transform of $X(t)$ and for its reconstruction, $X(t)$ is the inverse Fourier Transform

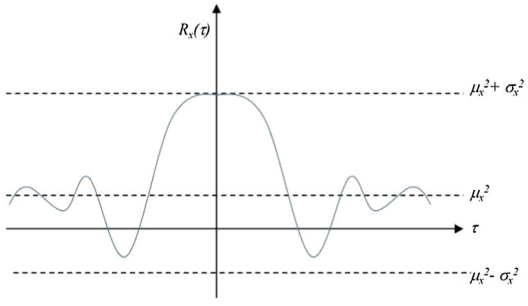

Fig. 17. Autocorrelation function.

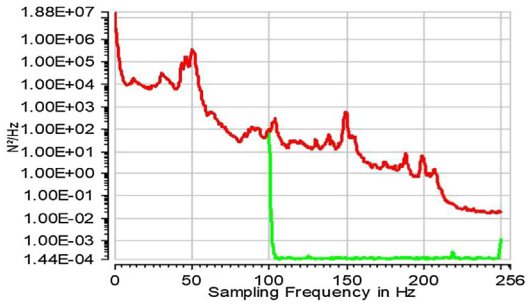

Fig. 18. PSD of the raw signal filtered at 100 Hz.

of $X(w)$ as represented by Eqs. (39) and (40) respectively:

$$X(w) = \frac{1}{2\pi}\int_{-\infty}^{\infty} X(t)e^{-iwt}dt. \tag{39}$$

$$X(t) = \int_{-\infty}^{\infty} X(t)e^{-iwt}dw. \tag{40}$$

For a stationary random process, the Fourier transform does not exist for the following condition:

$$\int_{-\infty}^{\infty} |X(w)|\, dt < \infty. \tag{41}$$

The Fourier transform of the autocorrelation function $Rx(\tau)$ exists. If this function is normalized to a zero-mean value, condition (41) is met. The forward and inverse Fourier transform are given by Eq. (42) and (43).

$$S_x(w) = \frac{1}{2\pi}\int_{-\infty}^{\infty} R_x(\tau)e^{-iwt}d\tau, \tag{42}$$

$$R_x(\tau) = \int_{-\infty}^{\infty} X(e)e^{-iwt}dw, \tag{43}$$

where $Sx(w)$ is the spectral density of the normalized function $X(t)$. When $\tau = 0$, Eq. (42) changes to:

$$E[X^2] = R_x(0) = \int_{-\infty}^{\infty} S_x(w)dw = \sigma_x^2. \tag{44}$$

Negative frequencies are excluded because they do not have a physical meaning. Changing the two-sided spectral density $S_x(w)$ into an equivalent one-sided spectral density $W_x(f)$, we have:

$$E[X^2] = \sigma_x^2 = \int_0^{\infty} W_x(f)df, \tag{45}$$

where the power spectral density $W_x(f)$ is given as:

$$W_x(f) = 4\pi S_x(w), \tag{46}$$

and

$$f = \frac{w}{2\pi}. \tag{47}$$

If a stationary random process $X(t)$ is derived one and two times, we have:

$$S_{\dot{x}}(w) = w^2 S_x(w), \tag{48}$$

$$W_{\dot{x}}(f) = (2\pi)^2 f^2 W_x(w), \tag{49}$$

$$\sigma_{\dot{x}}^2 = \int_{-\infty}^{\infty} S_{\dot{x}}(w)dw = \int_{-\infty}^{\infty} w^2 S_x(w)dw = (2\pi)^2 \int_{-\infty}^{\infty} f^2 W_x(f)df, \tag{50}$$

$$S_{\ddot{x}}(w) = w^4 S_x(w), \tag{51}$$

$$W_{\ddot{x}}(f) = (2\pi)^4 f^4 W_x(f), \tag{52}$$

$$\sigma_{\ddot{x}}^2 = \int_{-\infty}^{\infty} S_{\ddot{x}}(w)dw = \int_{-\infty}^{\infty} w^4 S_x(w)dw = (2\pi)^4 \int_{-\infty}^{\infty} f^4 W_x(f)df. \tag{53}$$

If the spectral density has only narrow-band frequencies, the process is called narrow-band. If the spectral density covers a broad-band of frequencies, the process is known as broad-band, such as the behaviour

of white noise. The *PSD* is normally represented using a log-log scale.

3.3. Review of damage rules and life prediction methods

Although the first study on fatigue in metallic materials was carried out around 1829 in Germany on mine scaffoldings,and Wöhler proposed a curve to represent the failure of railway axles in the 19th century, there is still a great deal of development work needed to propose damage rules. The most widely used damage approach is the Minerś damage rule,although Rognin et al. [32] concluded that the Minerś life prediction is greater than the experimental getting a non-conservative estimation for low cycle fatigue. Experimental results have demonstrated that during the fatigue process there is an effect on load sequence [33,34,32,35–38] and a number of approaches have been proposed taking into account the load interaction,some of which modify the SN curve or predict the fatigue life based on tensile properties [39,11,40]. Wormsen et al. [41] proposed a procedure to estimate SN data for high cycle fatigue for low alloy forged steel used in the subsea industry with tensile strength or hardness.

This review section provides a comprehensive updated summary of the recent advances in fatigue analysis based on the assumption that most of the damage models can be used in different applications. Further, a summary of the models introduced after the early 2000s until the beginning of 2019 is presented in this section, which has been split into Continuum Damage Approaches, multiaxial and energy methods and artificial neural network approaches.Early achievements are only briefly discussed as they have been reviewed in [42,43].

In Yang and Fatemi [42] the phenomenological mechanisms and quantification of the damage process are reviewed. While in a material and structure in engineering the damage is related to a reduction of supporting failure, in thermodynamics the entropy increases; the selection of the method therefore depends on the capabilities of the specimen being tested, if a mechanical measure is selected the result could be nondestructive or destructive, in the case of a measure with physical parameter result in an indirect measure giving a non-destructive method as X-radiography, Optical Holography, Material density, Acoustic Emission, Thermometric Measurements, Potential and Eddy current techniques, Ultrasonic Technique, Magnetic Field Methods combined with the Preisach hysteresis model can be used to evaluate the fatigue progress [44]. Based on ratchet strain and normal stress on the critical plane [45] defined a fatigue indicator parameter modeling with a microstructure sensitive, to find the microstructural growth and small cracks [46]. Fatemi and Yang [43] presented a summary of the damage approaches between the earlies from 1970s to 1990s, summarizing 56 damage models according to the following categories: linear damage rules, life curve modification methods, hybrid theories, nonlinear damage curve and two-stage linearization approaches, approaches based on the crack growth concept, continuum damage mechanics models and theories based on energy [47].

Some proposed models are mainly modifications of previous ones. Luo et al. [48] introduced a model modifying the evolution rule based on strain energy density to include plasticity. Jahed and Varvani-Farahani [49] proposed a model using energy based fatigue properties and in Jahed et al. [50] extended its capability to non-proportional loading using the incremental cyclic plasticity of Garud. Martinez et al. [51] presented a plastic damage model based on the Barcelona model. Calvo et al. [52] proposed a modification of the Liu damage model for a probabilistic formulation [53]. Bracessi et al. [54] established an innovative procedure for a model approach in frequency domain stress. Bolchoun et al. [55] evaluated thin-walled magnesium welds using a modification of the Rainflow cycle counting taking into account an interpolation of pure torsional and pure axial Wöhler curves. Lu et al. [56] proposed a universal criterion in multiaxial 2d cyclic loading based on a strain parameter, which depends on the type of failure. Liu and Yan [57] presented a method to evaluate fatigue under low cycle non-proportional loading, modifying the modified Wöhler curve methods to consider the multiaxility effect. Chen et al. [58] proposed a variable amplitude multiaxial fatigue life prediction based on the maximum damage parameter range. Correia et al. [59] proposed a generalization of the Castillo et al. [60] probabilistic fatigue model considering a generic parameter. In 2018, Ottosen et al. [61] proposed a modification to the multiaxial fatigue criterion [62] to consider stress gradient effects. Carpinteri et al. [63] reformulated the frequency domain critical plane criterion for multiaxial random loading. Pavlou [64] presented a new theory of macroscopic fatigue damage called the SN fatigue damage envelope, which uses the SN curve to build a damage map. Gao and Moan [65] improved the fatigue damage estimation in mooring lines for bimodal non-Gaussian loads in the frequency domain. Benasciutti and Tovo [66] proposed a non-Gaussian version of narrow band approximation and TB through nonlinear transformation with the same RMS and load non-normality. Portugal et al. [67] implemented a hybrid variant of cyclic counting based on the Rainflow algorithm.

Aeran et al. [68] proposed a new damage model based on the S-N curve modified by the model parameter δ_i as shown in (54):

$$D_i = 1 - \left[1 - \frac{n_i}{N_i}\right]^{\delta_i} \tag{54}$$

Sun et al. [69] proposed a statistical model based on probabilistic properties and a linear Miner's rule as:

$$D_B = \sum_{i=1}^{m}\left(\sum_{j=1}^{n_i}\left(\frac{1}{N_{ij}}\right)^{a_i} - \frac{n_i}{N_i}\cdot\frac{N_i-\mu_i}{\mu_i}\right),\ N_f = \frac{1}{D_b}\cdot\sum_{i=1}^{m} n_i \tag{55}$$

where *DB* is fatigue damage, N_f is the predicted whole life, m is the number of load levels in one loading block, n_i is the cycle number under i load level, N_{ij} and N_i are random fatigue life, a_i is the index of i load level and μ_i is the mean value.

Aid et al. [70] based on the damage stress concept taking into account the damage evolution in random loading under the assumption that the plastic strain rate is proportional to the effective stress damage σ_{equiv},

$$D_i = \frac{\sigma_{(i)d} - \sigma_i}{\sigma_u - \sigma_i} = \frac{\sigma_{equiv} - \sigma_{i+1}}{\sigma_u - \sigma_{i+1}} \tag{56}$$

Liu and Mahadevan [39] proposed a nonlinear fatigue damage model based on the Palmgren-Miner rule taking into account the load dependency (57)

$$\sum_{i=1}^{k}\frac{n_i}{N_i} = \sum_{i=1}^{k}\frac{1}{\frac{A_i}{\omega_i} + 1 - A_i} \tag{57}$$

where ω_i and A_i are the loading cycle distribution and material parameters respectively.

[71] proposed a modification to the Miner damage rule leading to a nonlinear model,i.e.:

$$D = \sum_{i=1}^{n}\beta_i\frac{lnN_{fi}}{lnN_{f1}} = 1 \tag{58}$$

where β_i is the equivalent life fraction.

3.3.1. Continuum damage approach

Guo et al. [72] introduced a dissipation model for high cycle fatigue to describe the thermomechanical response. Xiao et al. [73] presented a continuum damage model for high cycle fatigue based on thermodynamic by Leimatre and Chaboche. Chen and Plumtree [74] used the ductility exhaustion to propose a fatigue damage accumulation model. Oller et al. [75] formulated a thermomechanical constitutive model using the finite element method. Dattoma et al. [76] proposed a model for life prediction based on a nonlinear continuum damage model where the parameters of fatigue limit and the parameters of the model are experimentally determined. Tang et al. [77] established a method combining continuum damage mechanics with a mesomechanical

model using a two-scale representative model to analyze fatigue damage evolution.

Holopainen et al. [78] proposed an extension of the Ottosen et al. [61] model for high cycle fatigue with arbitrary multiaxial loads, using a concept of endurance surface in the stress space. Liang et al. [79] presented a nonlinear continuum damage model taking into account the loading frequency, which was based on the accumulation and localization of dislocations.The damage evolution law for high cycle fatigue can be expressed as follows:

$$\dot{D} = \frac{\eta c E^{\frac{\eta}{2}} d^{\frac{\eta}{2}} e}{l^2 n^{\frac{\eta}{2}-1}} Y^{\frac{\eta}{2}-1\dot{Y}} \tag{59}$$

where d, e, l and n are the microstructure geometrical parameters, η, and c are material coefficients and E is the Young Modulus.

Shen et al. [80] proposed an approach on continuum damage mechanics coupling the damage variable in the constitutive model using the effective stress, i.e.:

$$\varepsilon_{ij} = \frac{1+\nu}{E}\left(\frac{\sigma_{ij}}{1-D}\right) - \frac{\nu}{E}\left(\frac{\sigma_{kk}\delta_{ij}}{1-D}\right) \tag{60}$$

where ν is the Poisson's ratio.

Constantinescu et al. [81] proposed a computational method to thermomechanical fatigue composed of a fluid flow simulating the heat exchange coefficients and thermofluxes, a transient thermal diffusion simulating heating and cooling,and mechanical computation to determine a low cycle fatigue criterion, and validated it on manifolds.

Tateishi et al. [82] proposed a damage mechanics model for low cycle fatigue life considering the ductile and cycle damage as:

$$D = D_{cyclic} + D_{ductile} = \begin{cases} \sum_i \frac{n_i}{N_i} + \frac{\Delta\varepsilon_{max} - \varepsilon_{pD}}{\varepsilon_f - \varepsilon_{pD}} \text{ if } \Delta\varepsilon_{max} > \varepsilon_{pD} \\ \sum_i \frac{n_i}{N_i} \text{ if } \Delta\varepsilon_{max} \leqslant \varepsilon_{pD} \end{cases} \tag{61}$$

In 2011, Rejovitzky and Altus [83] proposed a stochastic micromechanical fatigue model representing the damage morphology with stochastic sets. Grandcoin et al. [84] established a continuum damage model to correlate since the matrix microscale damage to crack nucleation at the macro-scale on rubbers. Eslami et al. [85] defined a micromechanical model for the prediction of multiaxial high cycle fatigue (HCF) considering parameters as macroscopic stresses grain size and orientation, the failure criterion function g, d, ϕ, $tetha$, ψ, $\sum$) is expressed by Eq. (62):

$$g\left(d, \phi, \theta, \psi, \sum\right) = \Gamma_c - \frac{T_a\left(\phi, \theta, \psi, \sum\right) - \tau_y^{\infty} - k \cdot d^{\frac{1}{2}}}{h} \geqslant 0 \tag{62}$$

3.3.2. Multiaxial and energy methods

Some proposals are based on the classical multiaxial fatigue models such as the maximum effective strain model, the maximum shear strain model, the Fatemi-Socie (FS) model, the Smith-Watson-Topper model and the Itoh model [86,87].De-guand and De-jun [88] proposed a path-independent parameter in multiaxial fatigue basedon a critical plane approach. Lin et al. [89] proposed a damage parameter for multiaxial fatigue considering strain and stress,also based on a critical plane approach. Zhong et al. [86] proposed a fatigue damage model based on the projection path on the π-plane. Mei et al. [90] proposed a multiaxial damage model based on the moment of load path.

In 2015, Meggiolaro and Pinho de Castro [91] proposed the Incremental Fatigue Damage methodology to evaluate the damage until 6D multiaxial loads. It can be expressed as follows:

$$D = \int_{-\sigma_a}^{+\sigma_a} -\frac{1}{b(\sigma+\sigma_a)}\left(\frac{\sigma+\sigma_a}{2\sigma_c}\right)^{-\frac{1}{b}} \cdot d\sigma = \left(\frac{\sigma+\sigma_a}{2\sigma_c}\right)^{-\frac{1}{b}} \Bigg|_{-\sigma_a}^{+\sigma_a} \tag{63}$$

In 2017, Meggiolaro and Pinho de Castr [92] proposed a new criterion of high cycle fatigue based on the parameter β, which depends on the non-linear combination of the shear stress amplitude ($\tau_{a,c}$), hydrostatic stress amplitude ($\sigma_{a,c}^H$) and the normal stress ($\sigma_{a,c}$). It is represented by (64):

$$\beta = \sqrt{\left(\frac{\sigma_{a,c}}{f_{-1}}\right)^2 + \left(\frac{\tau_{a,c}}{f_{-1}}\right)^2 + \left(\frac{\sigma_{a,c}^H}{f_{-1}}\right)^2} \tag{64}$$

Gao et al. [93] proposed a multiaxial random vibration fatigue damage parameter equivalent to the stress power spectral density (PSD), which is a combination of shear stress and normal PSD stress. The fatigue life of a structure under random loading is defined as:

$$N_T = \frac{1}{\upsilon \int_0^{\infty} \frac{p(S)}{N(S)} dS} \tag{65}$$

where υ represents the cycles and $p(S)$ is the probability density function and the fatigue damage from multiaxial random vibration can be modelled as:

$$D = N_T = \upsilon \int_{S_e K_{RMS}/K_f}^{\infty} p(S)/N(S_e K_f / K_{RMS}) dS \tag{66}$$

In 2017, Correia et al. [94] proposed a generalization of the Kohout-Věchetfatigue model for variables as stress, strain energy-based parameters and is given in (67):

$$\psi(N) = \psi_e\left(\frac{N+N_u}{N+N_e}\right)^{b'} = \psi^{ULCF}\left[\frac{(N+N_u)N_e}{N+N_e}\right]^{b'} = \psi^{UHCF}\left(\frac{1+N/N_u}{1+N/N_e}\right)^{b'} \tag{67}$$

where the parameters are; ψ_e is the fatigue limit, ψ^{ULCF} is the ultimate fatigue damage parameter for low cycle fatigue, and ψ^{UHCF} the ultimate fatigue damage for high cycle fatigue.

Benkabouche et al. [95] proposed the following nonlinear model for variable and multiaxial loads:

$$D_{i+1} = \frac{\sum_{i+1}^{eq} -\sigma_{eq}^{i+1max}}{\tau_u - \sigma_{eq}^{i+1max}} \tag{68}$$

where $\sum_{i+1}^{eq}$ is the damage stress amplitude.

Rege and Pavlou [96] presented a nonlinear model under variable amplitude loads, which only requires the $q(\sigma_i)$ parameter in addition to the fatigue material parameters, the process begins calculating the initial isodamage path, i.e.:

$$D_i = \left(\frac{logN_e - logN_i}{logN_e - log(n_{(i-1),(i)} + n_i)}\right)^{q(\sigma_i)} \tag{69}$$

$$q(\sigma_i) = (a\sigma_i)^b = \left(\frac{2\sigma_i}{\sigma_s}\right)^{-0.75} \tag{70}$$

In 2019, Zhu et al. [97] proposed a nonlinear damage introducing a damage function related to the isodamage curves. It can be expressed as follows (71):

$$D_i = \left(\frac{logN_e - logN_i}{logN_e - log(n_{(i-1),(i)} + n_i)}\right)^{(ilogn_i + slog\varepsilon_{a,i})} \tag{71}$$

where n_i is the number of cycles at σ_i $logn_{i-1,i}$ as follows:

$$logn_{i-1,i} = logN_e - \frac{logN_e - logN_i}{D_{i-1}^{\frac{1}{(ilogn_i + slog\varepsilon_{a,i})}}} \tag{72}$$

Kang et al. [98] proposed a thermomechanical fatigue damage model for variable temperatures and loadings, and defined an equivalent damage temperature for each loading cycle.With consideration to the total damage being the sum of mechanical and oxidation damage,

the mechanical damage was computed using the Smith-Watson-Topper model and the oxidation damage (D^{oxi}) with the Sehitoglu model, as shown in Eq. (73):

$$D^{oxi} = \frac{1}{N_f^{oxi}} = \left(\frac{h_{cr}\delta_o}{BF_p^{eff}\phi^{oxi}}\right)^{-\frac{1}{\beta}}\left(\frac{2\Delta\varepsilon_{mech}^{1+\frac{2}{\beta}}}{\dot{\varepsilon}^{1-\frac{a}{\beta}}}\right) \tag{73}$$

Parameters K_p^{eff} and ϕ^{oxi} are computed using Eq. (74) and (75) respectively.

$$K_p^{eff} = \frac{1}{t_c}\int_0^{t_c} D_o e^{\frac{-Q}{RT(t)}}dt \tag{74}$$

$$\phi^{oxi} = \frac{1}{t_c}\int_0^{t_c} e^{\left[-\frac{1}{2}\frac{\dot{\varepsilon}_{th}}{\dot{\varepsilon}_{meth}+1}\frac{}{\xi^{oxi}}\right]}dt \tag{75}$$

where h_{cr} is critical crack length, and δ_o and are material constants, and β and B are constant based on the total oxide growth. K_p^{eff} is effective oxidation and ϕ^{oxi} is a phasing factor. D_o is the diffusion coefficient for oxidation, Q is the energy for activation oxidation, R is the Universal gas constant, $T(t)$ is the temperature, tc is the cycle period and ε_{th} is the phasing sensitivity for the oxidation damage. The thermal strain ($\dot{\varepsilon}_{th}$) rate and mechanical strain ($\dot{\varepsilon}_{mech}$) rate.

In 2017, Lu et al. [99] proposed an approach for the definition of the critical plane and a new energy-based multiaxial parameter defined in terms of normal and shear strain energy contributions taking into account the influence of the Poisson effect. Li and Ince [100] proposed a unified frequency domain fatigue damage approach for complex random loads, for a number of *PSD* segments (k, ν) the applied number of segments is defined as:

$$n_{n,k} = f_j T_j P_{j,k} \tag{76}$$

where f_j is the central frequency and $P_{j,k}$ is the probability of the Rayleigh stress distributions for the $\nu - th$ PSD segment, the damage and total damage for each ν PSD position can be expressed as:

$$d = \sum_{j=1}^{v}\sum_{k=1}^{5}\frac{n_{j,k}}{N_{j,k}} \tag{77}$$

$$D = \sum_{i=1}^{u} d_i = \sum_{i=1}^{u}\sum_{j=1}^{v}\sum_{k=1}^{5}\frac{f_{i,j}T_i P_k}{C(S_{log}\cdot G_{rms_{i,j}\cdot E_{\mu k}})^{-b}} \tag{78}$$

Mamiya et al. [101] under the assumption that in low cycle fatigue σ_{Hmax} includes the effect of crack opening and any hardening or softening for the cyclic material response, to modify the cyclic property τ_f' is used the square root of the mean second invariant $J2m$ of the deviatoric stress, to get a fatigue model as follows:

$$\gamma_{aMPH} + \frac{k}{G}\sigma_{Hmax} = \frac{\tau_f' - \sqrt{J_{2m}}}{G}(2N_d)^{b_0} + \gamma_f'(2N_f)^{C_0} \tag{79}$$

where G is the shear modulus, and τ_f' , b_0 and γ_f' are the cyclic properties of the material.

Gao et al. [93] proposed a multiaxial random vibration fatigue parameter based on a critical plane damage parameter for multiaxial high cycle fatigue equivalent to stress power density, and validated it with thin-walled circular tube experiments.Wang and Yao [102] proposed a multiaxial fatigue parameter using the maximum shear strain plane as the critical plane. Li et al. [87] proposed a fatigue life approach for multiaxial loading in high cycle fatigue using a path-dependent factor, it is represented by Eq. (80),

$$F_h = \frac{\tau_{a,min}\tau_{a,w}}{\sigma_{eq}^2} \tag{80}$$

where $\tau_{a,min}$ and $\tau_{a,w}$ are the rotation degree of principal stress and stress length and are normalized by Von-Misses equivalent stress σ_{eq}.

Scott-Emuakpor et al. [103] developed an expression for equivalent stress in a multiaxial load condition, incorporating non-linear plastic stress-strain relations to apply it in the distortion energy theory. Wang and Xiao [104] proposed an elastoplastic flow model combined with nonlinear hardening. Djebli et al. [105] proposed a fatigue damage model based on transforming the SN curve to energy parameters, i.e.:

$$D = \frac{W_{equiv} - W_{i+1}}{W_u - W_{i+1}} \tag{81}$$

where W_{equiv}, W_i and W_u are the energies due to stress damage, applied stress and ultimate stress, respectively.

Lee et al. [106] developed a model to include a plastic strain energy density parameter to take into account temperature effect, which uses a tensile toughness w_o for a temperature dependent parameter. It is represented by Eq. (82):

$$\left(\frac{\Delta w_p}{C_w w_o}\right)^{\frac{1}{m}} N_f = 1 \tag{82}$$

Feng et al. [107] proposed an energy dissipation fatigue prediction model for multiaxial fatigue for a known strain path. Park et al. [108] developed a fatigue life prediction for marine structures with a combined probability density function as (83):

$$D = \frac{Tf_{pf}}{\bar{a}}(2\sqrt{2m_0})^m\left[\frac{C_G}{\sqrt{\pi}}\sigma_G^m\Gamma\left(\frac{m+1}{2}\right) + C_{R1}\sigma_{R1}^m\Gamma\left(\frac{m+1}{2}\right) + C_{R2}\Gamma\left(\frac{m+1}{2}\right)\right] \tag{83}$$

3.3.3. Artificial neural networks

The last classification of methods reviewed in this section is Artificial Neural Network(ANN) methods, which can be used to classify and estimate the damage [109]. Figueria Pujol and Andrade Pinto [110] proposed a fatigue life prediction approach using an ANN. Durodola et al. [111] presented an ANN to consider the effect of mean stress in fatigue life prediction in the frequency domain. Zhu et al. [112] proposed a probabilistic model to predict damage in an orthotropic steel deck using a Bayesian network. Fathalla et al. [113] built an ANN for the diagnosis of the fatigue life of a service road bridge. Franulović [114] implemented a genetic algorithm to describe the elastoplastic behavior in low cycle fatigue. Shabbir and Omenzetter [115] combined a genetic algorithm with a sequential niche technique to minimize the error between the model and structure model. Jimenez-Martinez and Alfaro-Ponce [116] proposed a fatigue damage evaluation using an ANN taking into account load sequences and temperature in fatigue processes. Kim et al. [117] proposed a fatigue analysis method using an ANN to include the effect of wind speed and frequency in the stress function. Müller [118] performed fatigue evaluation based on response surface modelling using Latin Hypercube Sampling and an ANN.Chin Wong and Kim [119] developed an ANN model to predict the vortex induced vibration fatigue damage of a top tensioned riser. Piedas Lopes and Ebecken [120] evaluated the fatigue damage of fixed offshore structures using a feedforward backpropagation neural network. Li et al. [121] proposed an approach for wide banded fatigue prediction of catenary mooring lines based on an ANN.

Bukkapatnam and Sadananda [122] proposed a model of fatigue crack growth based on a unified approach that included the load ratio, short cracks, shielding of dislocation overload, underload and surface crack effects and considered the stress and peak stress intensity parameters. The parametrization was performed using a genetic algorithm with an extended sigmoidal function to capture the fatigue response, it is represented by Eq. (84):

$$\frac{dA}{dN} = C_1\psi(\Delta K, K_{max}) \tag{84}$$

where

$$\psi(\Delta K, K_{max}) = (s_0 - 2\gamma(\Delta K, \Delta K_0, K_{max}))K_{max}^n \tag{85}$$

and

$$\gamma(\Delta K, \Delta K_0, K_{max}) = \frac{e^{b(\Delta K_0 - \Delta K)^m}}{e^{b(\Delta K_0 - \Delta K)^m} + e^{b(\alpha_1 K_{max} + \alpha_2 \Delta k + \alpha_3 \Delta K_0)^m}} \tag{86}$$

Low [123] developed an approach for the rainflow fatigue damage arising from a Gaussian bimodal for the damage ratio L. It can be expressed as follows:

$$L = [b_1\sigma_{X_{HF}} + b_2\sigma_{X_{HF}}^2 - (b_1 + b_2)\sigma_{X_{HF}}^3 + \sigma_{X_{HF}}^m](\beta - 1) + 1 \tag{87}$$

where the parameters b_1 and b_2 are:

$$b_1 = (1.111 + 0.7241\ \text{m} - 0.0724\ \text{m}^2)\beta^{-1} + (2.403 - 2.483\ \text{m})\beta^{-2} \tag{88}$$

$$b_2 = (-10.45 + 2.65\ \text{m})\beta^{-1} + (2.607 + 2.63\ \text{m} - 0.0133\ \text{m}^2)\beta^{-2} \tag{89}$$

Kim et al. [124] developed a fatigue model for a wide-band spectrum using an ANN trained with different wide-band spectra and using the Rainflow counting method.

3.4. Damage analysis on offshore structures

In offshore structures, the structural responses due to the waves are Gaussian and narrow-banded [27]. To modulate the damage, a variable amplitude loading can be expressed as is shown in Eq. (90).

$$D = \sum_{i=1}^{k} \frac{n_i}{N_{f,i}}, \tag{90}$$

where n_i is the number of load cycles applied at amplitude $S_{a,i}$, $N_{f,i}$ is the number of cycles until failure in the i_{th} load level and k is the total number of blocks. The number of cycles until failure at the amplitude $S_{a,i}$ can be expressed as follows:

$$N_{f,i} = \frac{1}{2}\left(\frac{S_{a,i}}{S'_f}\right)^{\frac{1}{b}}, \tag{91}$$

where $S'f$ and b are the fatigue strength coefficient and exponent respectively. For $m = -1/b$ and $A = 0.5(S'f)m$ using Eq. (92), we can determine N_f for a given $S_{a,i}$ as follows:

$$N_{f,i} = A \times S_{a,i}^{-m}, \tag{92}$$

In a narrow-band stress process $S(t)$, cycle counting can be performed using the Rainflow process or by counting the number of peaks n_i in the window ΔS. For a peak counting process, the probability (f_i) that a stress amplitude occurs is given by:

$$f_i = \frac{n_i}{\sum_{i=1}^{k} n_i}, \tag{93}$$

The damage can be expressed as:

$$D = \sum_{i=1}^{k} \frac{n_i}{N_{f,i}} = \sum_{i=1}^{k} \frac{f_i \sum_{i=1}^{k} n_i}{N_{f,i}} = \sum_{i=1}^{k} n_i \frac{\sum_{i=1}^{k} f_i}{AS_{a,i}^{-m}}, \tag{94}$$

$$D = \frac{1}{A}\sum_{i=1}^{k} n_i \sum_{i=1}^{k} f_i S_{a,i}^m, \tag{95}$$

defining

$$E(S_a^m) = \sum_{i=1}^{k} f_i S_i^m, \tag{96}$$

$$D = \frac{\sum_{i=1}^{k} n_i}{A} E(S_a^m). \tag{97}$$

Considering that the *PDF* is a continuous random variable, the expected S_a^m is:

$$E(S_a^m) = \int_0^\infty S_a^m f_{Sa}(S_a) dS_a. \tag{98}$$

Defining the common Weibull distribution with the scale parameter (α), shape parameter (β) and gamma function (Γ), the cumulative function and Weibull distribution are given as:

$$F_{Sa}(S_a) = 1 - exp\left[-\left(\frac{S_a}{\alpha}\right)^\beta\right], \tag{99}$$

$$E(S_a^m) = \alpha^m \Gamma\left(\frac{m}{\beta} + 1\right). \tag{100}$$

When $\beta = 2$, the distribution simplifies to the Raleigh distribution for an RMS of σ_s, as shown in Eq. (101):

$$\alpha = \sqrt{2\sigma_s}, \tag{101}$$

and

$$E(S_a^m) = (\sqrt{2\sigma_s}^m)\Gamma\left(\frac{m}{\beta} + 1\right). \tag{102}$$

The expected total fatigue damage D_{NB} for $\sigma_s = \sqrt{M_o}$,

$$D_{NB} = \frac{\sum_{i:1}^{k}}{A} E(S_a^m) = \frac{E[0^+] \times T}{A}(\sqrt{2M_o}^m)\Gamma\left(\frac{m}{\beta} + 1\right). \tag{103}$$

For a wide-band Gaussian, the damage proposed by Wirsching and Light is based on the narrow-band damage process and is applied to the Rainflow correction factor (ζ_w), as shown in Eq. (104):

$$D_{WB,Wirshing} = \zeta_w D_{NB}. \tag{104}$$

The correction factor depends on the slope of the $S - N$ curve (m) and the spectral width parameter (λ):

$$\zeta_s = a_s + [1 - a_s](1 - \lambda)^{bw}. \tag{105}$$

Parameters a_s and b_s are computed using Eq. (106) and (107) respectively

$$a_s = 0.926 - 0.033m, \tag{106}$$

$$b_s = 1.587m - 2.323. \tag{107}$$

The damage for a wind band Gaussian process proposed by Oritz and Chen is given as:

$$D_{WB,Oritz} = \zeta_o D_{NB}, \tag{108}$$

where ζ and k are described by Eqs. (109) and (110) respectively,

$$\zeta_o = \frac{1}{\gamma}\sqrt{\frac{M_2 M_k}{M_o M_{k+2}}}. \tag{109}$$

$$k = \frac{2.0}{m}, \tag{110}$$

Finally, Dirlik proposed a damage model for the PDF of Rainflow amplitude $F_{Sa}(Sa)$, Eq. (111) and the amplitude is described in Eq. (112):

$$D_{WB,Dirlik} = \frac{E[P]\tau}{A}\int_0^\infty S_a^m f_{Sa}(S_a) dS_a, \tag{111}$$

$$f_{Sa}(S_a) = \frac{D_1}{2\sqrt{M_o}Q} e^{-\frac{Z}{Q}\times S_a} + \frac{D_2 \times Z}{2\sqrt{M_o}R^2} e^{-\frac{Z}{2R^2}\times S_a^2} + \frac{D_3 \times Z}{2\sqrt{M_o}} e^{-\frac{Z}{2}\times S_a^2}, \tag{112}$$

where the parameters are defined by:

$$z = \frac{1}{2\sqrt{M_o}}, \tag{113}$$

$$\gamma = \frac{M_2}{\sqrt{M_o M_4}}, \tag{114}$$

$$X_m = \frac{M_1}{M_o}\sqrt{\frac{M_2}{M_4}}, \tag{115}$$

$$D_1 = \frac{2(X_m - \gamma^2)}{1+\gamma^2}, \tag{116}$$

$$R = \frac{\gamma - X_m - D_1^2}{1 - \gamma - D_1 - D_1^2}, \tag{117}$$

$$D_2 = \frac{1 - \gamma - D_1 + D_1^2}{1 - R}, \tag{118}$$

$$D_3 = 1 - D_1 - D_2, \tag{119}$$

$$Q = \frac{1.25(\gamma - D_3 - D_2 \times R)}{D_1}. \tag{120}$$

4. Accelerated test

The measurement period is usually not long enough to be used directly in a test. The main target for the extrapolated signals is based on time measurement restriction problems such as synchronicity, spikes, and drift of the measurement devices. The information acquired is then analysed to eliminate unnecessary information such as noise. To achieve this, filters are utilized and statistical analyses are performed. For structural analysis, it is necessary to use a low pass filter of 100 Hz [125]. To evaluate the changes after the application of the filter, it is better to use cycle counting tools and to evaluate the pseudo damage using the linear damage rule [125]. The results of this evaluation are shown in Fig. 19. Based on the analysis, the spectrum is built via cycle counting (Fig. 19)a and it is transformed into the spectrum (Fig. 19b).

To reduce the test time, low amplitude loads can be omitted because 89% of the time test these loads only generate 8% of the total damage [126]. These authors proposed and standardized a spectrum based on the relationship:

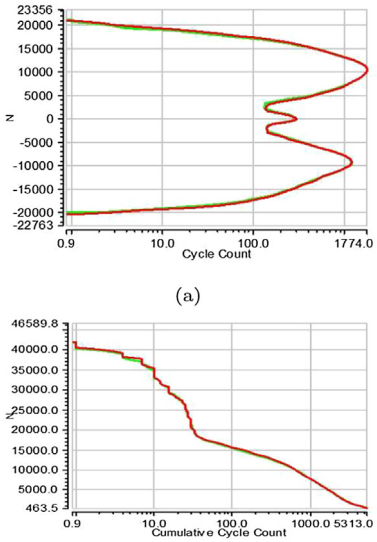

Fig. 19. Statistical analysis of the raw data compared with the filtered signal (a) Cycle counting, (b) Cumulative cycle count.

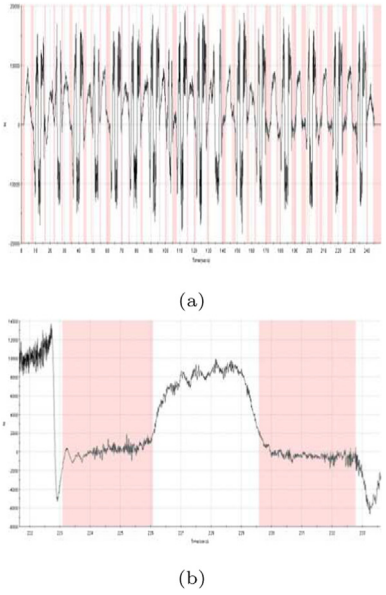

Fig. 20. Selection of some areas from the filtered raw data time history, (a) 0–249.9 s, (b) zoom between 221.7 and 233.6 s.

$$W(f) = AH_s^{2\varphi}\frac{exp\left[\frac{-1050}{(2\pi T_d f)^4}\right]}{T_d^4(2\pi f)^5\left[\left\{1-\left(\frac{f}{f_n}\right)^2\right\}^2 + \left\{\frac{2\zeta f}{f_n}\right\}^2\right]}, \tag{121}$$

where $W(f)$ is the spectral density, A is the scale factor, H_s is the significant wave height, φ is the stress variation with sea state, and T_d is the dominant wave period.

Test responses and desired signals must be evaluated. The correlation between the results in the lab is essential because the main aim of accelerated tests is to reproduce the same failures to prevent them in the future. The test components are more extensive and include all the variables for the load conditions. Low load amplitudes are omitted as shown in Fig. 20. Fig. 20a shows all the areas that are eliminated and Fig. 20b is a detail view.

Fig. 21 summarizes the spectrums of all the strategies to extrapolate

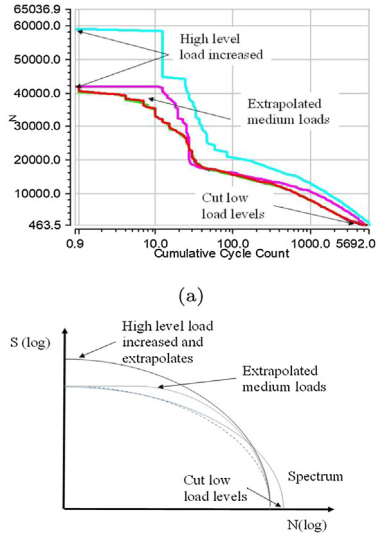

Fig. 21. Spectrum of the time histories (a) summary of the reduction of the time test, (b) schematic of accelerated test.

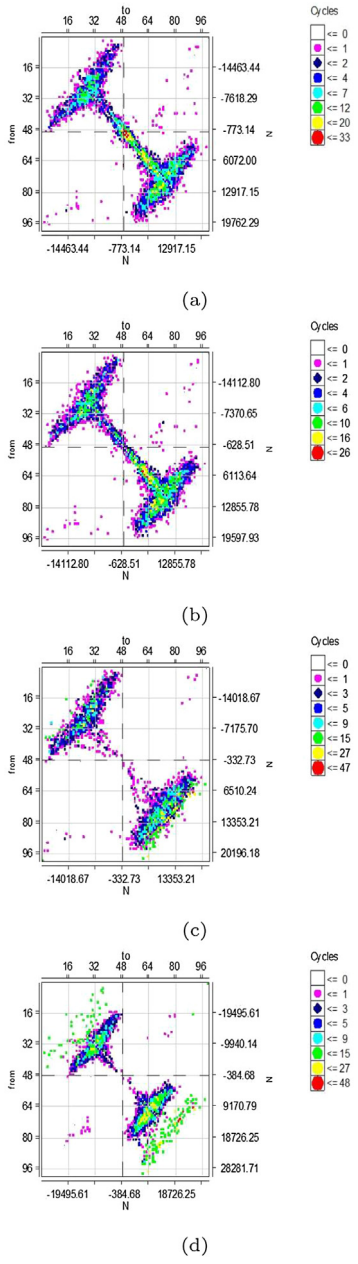

Fig. 22. Rainflow matrix (a) raw data, (b) cut filtered signal, (c) medium load increase, (d) high load increase.

the time histories. The raw filtered data could be cut below the load level to reduce the testing time. The signal can increase the medium and high loads and the test is accelerated, thereby reducing the original time and increasing the damage. This reduces the total time of the test for the duration. Fig. 21 depicts the schematic techniques used to accelerate the test.

Another potential representation is to use the Matrix Rainflow. Fig. 22a shows the original signals, filtered signal (Fig. 22b), the increasing high loads (Fig. 22c) and the increase in the number of reversals in the high loads inclusive of the maximum loads of the raw data. The difference is seen in the time histories where the loads for medium and high loads are extrapolated.

5. Summary

Experimental evaluation is mandatory to analyse the scattering of the manufacturing process, materials and offshore structures including the random responses from the load of the environment to prevent failures during the service life. Offshore structures suffer damage from internal loads in addition to external sources such as the wind, waves and sea currents. The damage approach used depends on the process generated by the random loads and the irregularity of the time history. The main models used for wide-band Gaussian processes are the Dirlik, Oritz and Chen. The Wirsching and Light model has also been proposed.

The aggressive environment of offshore structures accelerates damage through corrosion. Control of external corrosion can be achieved using alloying elements, coatings, cathodic protection, linings and metal cladding. Metal alloys must be evaluated to reduce corrosion without reducing their fatigue strength.

Extrapolation can be performed in three main ways; increasing high loads or medium loads, as well as cutting low load levels. It changes the spectrum thereby reducing the time history. Accelerated fatigue can be applied to reduce the time for testing because most of the loads in a time history only account for a small portion of the damage. It is possible to use a standardized spectrum but it must meet not only the load conditions, but also must include environmental effects. Accelerated testing can be performed using a resonance test equipment and the resonance phenomenon is used to reduce the energy required to induce the amplitude, this test must include the sea water by modifying the amount of salt present in order to increase the corrosion velocity.

The cycle counting methods show the damage and repetitions for each amplitude. It can assist in the generation of a spectrum to develop a test or to extrapolate the signal to accelerate a test. The first step in the statistical analysis process is to apply a filter to eliminate unnecessary amplitudes generated by noise during the measurement. Uncertainties from internal and external loads are included in the time history while the scatter of materials and design are included in the S-N curves. To prevent failures during its operation, high design factors are defined because additional loads can be included to perform measurement with equipment on the platforms. In the case of pipelines, probes are introduced to acquire geophysical records. The tool is fixed in the pipe to measure pressure and temperature with the well flow or the measurement is recorded in the tool and subsequently recovered.

Although the fundamental fatigue analysis seems to be similar to that of other industries such as the automotive industry, the durability evaluation changes based on the variable amplitude loads represented by its spectrum and are directly evaluated in comparison with the material properties. In an offshore environment, it is necessary to understand the irregularity of the loads and to apply a damage model depending on the type of random variables such as wind, wave loads and corrosion effect.

More effort is required in the study of fatigue damage in offshore industries to generate correction factors to address nonlinearities, thereby preventing overdesign and producing reliable results. A standardized spectrum can be proposed such as in the case of Hartt and Lin, but it depends on the type of structure and the location. To consider the temperature effects in addition to the generation of a direct contribution of stress on the component, the uncertainties of random loads depend on the offshore location.

References

[1] Karimirad M. Offshore energy structures. Springer International Publishing; 2014.
[2] Hirdaris S, Bai W, Dessi D, Ergin A, Gu X, Hermundstad O, et al. Loads for use in the design of ships and offshore structures. Ocean Eng 2014;78:131–74.
[3] Pinheiro BdeC, Pasqualino IP. Fatigue analysis of damaged steel pipelines under cyclic internal pressure. Int J Fatigue 2009;31(5):962–73.
[4] Song X, Wang S. A novel spectral moments equivalence based lumping block method for efficient estimation of offshore structural fatigue damage. Int J Fatigue 2019;118:162–75.
[5] Dallyn P, El-Hamalawi A, Palmeri A, Knight R. Experimental testing of grouted connections for offshore substructures: a critical review. Structures 2015;3:90–108.
[6] Chen L, Basu B. Fatigue load estimation of a spar-type floating offshore wind turbine considering wave-current interactions. Int J Fatigue 2018;116:421–8.
[7] Mansor N, Abdullah S, Ariffin A, Syarif J. A review of the fatigue failure

mechanism of metallic materials under a corroded environment. Eng Fail Anal 2014;42:353–65.
[8] Horstmann M, Gregory J, Schwalbe K-H. Geometry effects on corrosion-fatigue in offshore structural steels. Int J Fatigue 1995;17(4):293–9.
[9] Adedipe O, Brennan F, Kolios A. Review of corrosion fatigue in offshore structures: present status and challenges in the offshore wind sector. Renew Sustain Energy Rev 2016;61:141–54.
[10] Banvillet A, Lagoda T, Macha E, Nieslony A, Palin-Luc T, Vittori J-F. Fatigue life under non-Gaussian random loading from various models. Int J Fatigue 2004;26(4):349–63.
[11] Jimenez M, Martinez J, Figueroa U, Altamirano L. Estimated s-n curve for nodular cast iron: a steering knuckle case study. Int J Automotive Technol 2014;15(7):1197–204.
[12] Jimenez M. DURABILITY TESTS: statistical analysIs for variable amplitude loads. Trans Can Soc Mech Eng 2017;41(5):910–21.
[13] TL L, J P, R H, M B. Fatigue testing and analysis. Elsevier ButterWorth-Heinemann; 2005.
[14] Hoell S, Omenzetter P. Optimal selection of autoregressive model coefficients for early damage detectability with an application to wind turbine blades. Mech Syst Signal Process 2016;70–71:557–77.
[15] Jacob A, Oliveira J, Mehmanparast A, Hosseinzadeh F, Kelleher J, Berto F. Residual stress measurements in offshore wind monopile weldments using neutron diffraction technique and contour method. Theoret Appl Fract Mech 2018;96:418–27.
[16] Drumond GP, Pasqualino IP, Pinheiro BC, Estefen SF. Pipelines, risers and umbilicals failures: a literature review. Ocean Eng 2018;148:412–25.
[17] Devaney RJ, O'Donoghue PE, Leen SB. Experimental characterisation and computational modelling for cyclic elastic-plastic constitutive behaviour and fatigue damage of x100q for steel catenary risers. Int J Fatigue 2018;116:366–78.
[18] Wormsen A, Fjeldstad A, Kirkemo F, Muff AD, Reinås L, Macdonald KA. Fatigue analysis of low alloy steel forgings used in the subsea industry. Int J Fatigue 2017;96:43–66.
[19] O'Halloran S, Connaire A, Harte A, Leen S. Modelling of fretting in the pressure armour layer of flexible marine risers. Tribol Int 2016;100:306–16. 42nd Leeds-Lyon Symposium on Tribology- Surfaces and Interfaces: Mysteries at Different Scales.
[20] Ramsamooj D, Shugar T. Modeling of corrosion fatigue in metals in an aggressive environment. Int J Fatigue 2001;23:301–9.
[21] Modarres-Sadeghi Y, Mukundan H, Dahl J, Hover F, Triantafyllou M. The effect of higher harmonic forces on fatigue life of marine risers. J Sound Vib 2010;329(1):43–55.
[22] Gracia LD, Wang H, Mao W, Osawa N, Rychlik I, Storhaug G. Comparison of two statistical wave models for fatigue and fracture analysis of ship structures. Ocean Eng 2019;187:106161.
[23] Cerveira F, Fonseca N, Pascoal R. Mooring system influence on the efficiency of wave energy converters. Int J Mar Energy 2013;3–4:65–81 special Issue – Selected Papers - EWTEC2013.
[24] Videiro PM, Giraldo JSM, de Sousa FJM, dos Santos CMPM, Sagrilo LVS. Long-term analysis using a scatter diagram key region to evaluate the extreme response of steel risers. Mar Struct 2019;64:322–40.
[25] Ma J, Zhou D, Han Z, Zhang K, Bao Y, Dong L. Fluctuating wind and wave simulations and its application in structural analysis of a semi-submersible offshore platform. Int J Naval Archit Ocean Eng 2019;11(1):624–37.
[26] Mukundan H, Modarres-Sadeghi Y, Dahl J, Hover F, Triantafyllou M. Monitoring viv fatigue damage on marine risers. J Fluids Struct 2009;25(4):617–28. bluff Body Wakes and Vortex-Induced Vibrations (BBVIV-5).
[27] Gao Z, Moan T. Frequency-domain fatigue analysis of wide-band stationary Gaussian processes using a trimodal spectral formulation. Int J Fatigue 2008;30(10):1944–55.
[28] Karlsson J, Podgórski K, Rychlik I. The laplace multi-axial response model for fatigue analysis. Int J Fatigue 2016;85:11–7.
[29] Heuler P, Klätschke H. Generation and use of standardised load spectra and load–time histories. Int J Fatigue 2005;27(8):974–90. cumulative Fatigue Damage Conference - University of Seville 2003.
[30] Rychlik I, Gupta S. Rain-flow fatigue damage for transformed Gaussian loads. Int J Fatigue 2007;29(3):406–20.
[31] Marsh G, Wignall C, Thies PR, Barltrop N, Incecik A, Venugopal V, et al. Review and application of rainflow residue processing techniques for accurate fatigue damage estimation. Int J Fatigue 2016;82:757–65.
[32] Rognin F, Abdi F, Kunc V, Lee M, Nikbin K. Probabilistic methods in predicting damage under multi-stage fatigue of composites using load block sequences. Procedia Eng 2009;1(1):55–8. mesomechanics 2009.
[33] Gladskyi M, Fatemi A. Notched fatigue behavior including load sequence effects under axial and torsional loadings. Int J Fatigue 2013;55:43–53.
[34] Harbour RJ, Fatemi A, Mars WV. Fatigue life analysis and predictions for nr and sbr under variable amplitude and multiaxial loading conditions. Int J Fatigue 2008;30(7):1231–47.
[35] Yin F, Fatemi A, Bonnen J. Variable amplitude fatigue behavior and life predictions of case-hardened steels. Int J Fatigue 2010;32(7):1126–35.
[36] Ben-Amoz M. Cumulative damage model based on two-mode fatigue damage bounds. Mater Sci Eng A 2009;504(1):114–23.
[37] Memon IR, Zhang X, Cui D. Fatigue life prediction of 3-d problems by damage mechanics with two-block loading. Int J Fatigue 2002;24(1):29–37.
[38] Rejovitzky E, Altus E. Non-commutative fatigue damage evolution by material heterogeneity. Int J Fatigue 2012;37:54–9.
[39] Liu Y, Mahadevan S. Multiaxial high-cycle fatigue criterion and life prediction for metals. Int J Fatigue 2005;27(7):790–800.
[40] Shamsaei N, McKelvey SA. Multiaxial life predictions in absence of any fatigue properties. Int J Fatigue 2014;67:62–72. multiaxial Fatigue 2013.
[41] Wormsen A, Avice M, Gulbrandsen E, Reinås L, Macdonald KA, Muff AD. Base material fatigue data for low alloy forged steels used in the subsea industry. part 2: Effect of cathodic protection. Int J Fatigue 2015;80:496–508.
[42] Yang L, Fatemi A. Cumulative fatigue damage mechanisms and quantifying parameters: a literature review. J Test Eval 1998;26(2):89–100.
[43] Fatemi A, Yang L. Cumulative fatigue damage and life prediction theories: a survey of the state of the art for homogeneous materials. Int J Fatigue 1998;20(1):9–34.
[44] Vandenbossche L, Dupré L, Melkebeek J. Preisach-based magnetic evaluation of fatigue damage progression. J Magn Magn Mater 2005;290–291:486–9. proceedings of the Joint European Magnetic Symposia (JEMS' 04).
[45] Zhang M, Neu R, McDowell D. Microstructure-sensitive modeling: application to fretting contacts. Int J Fatigue 2009;31(8):1397–406.
[46] McDowell DL. Multiaxial small fatigue crack growth in metals. Int J Fatigue 1997;19(93):127–35.
[47] Liao D, Zhu S-P. Energy field intensity approach for notch fatigue analysis. Int J Fatigue 2019;127:190–202.
[48] Luo C, Chattopadhyay A. Prediction of fatigue crack initial stage based on a multiscale damage criterion. Int J Fatigue 2011;33(3):403–13.
[49] Jahed H, Varvani-Farahani A. Upper and lower fatigue life limits model using energy-based fatigue properties. Int J Fatigue 2006;28(5):467–73. selected papers from the 7th International Conference on Biaxial/Multiaxial Fatigue and Fracture (ICBMFF).
[50] Jahed H, Varvani-Farahani A, Noban M, Khalaji I. An energy-based fatigue life assessment model for various metallic materials under proportional and non-proportional loading conditions. Int J Fatigue 2007;29(4):647–55.
[51] Martinez X, Oller S, Barbu L, Barbat A, de Jesus A. Analysis of ultra low cycle fatigue problems with the barcelona plastic damage model and a new isotropic hardening law. Int J Fatigue 2015;73:132–42.
[52] Calvo S, Canales M, Gómez C, Valdés J, Núñez J. Probabilistic formulation of the multiaxial fatigue damage of liu. Int J Fatigue 2011;33(3):460–5.
[53] Liu Y, Mahadevan S. Stochastic fatigue damage modeling under variable amplitude loading. Int J Fatigue 2007;29(6):1149–61.
[54] Braccesi C, Cianetti F, Tomassini L. An innovative modal approach for frequency domain stress recovery and fatigue damage evaluation. Int J Fatigue 2016;91:382–96. variable Amplitude Loading.
[55] Bolchoun A, Baumgartner J, Kaufmann H. A new method for fatigue life evaluation under out-of-phase variable amplitude loadings and its application to thin-walled magnesium welds. Int J Fatigue 2017;101:159–68. fatigue Assessment of Welded Joints by Modern Concepts.
[56] Lu C, Melendez J, Martínez-Esnaola J. A universally applicable multiaxial fatigue criterion in 2d cyclic loading. Int J Fatigue 2018;110:95–104.
[57] Liu B, Yan X. A new method for studying the effect of multiaxial strain states on low cycle non-proportional fatigue prediction. Int J Fatigue 2018;117:420–31.
[58] Chen H, Shang D-G, Tian Y-J, Liu J-Z. Fatigue life prediction under variable amplitude axial–torsion loading using maximum damage parameter range method. Int J Press Vessels Pip 2013;111–112:253–61.
[59] Correia J, Apetre N, Arcari A, Jesus AD, Muñiz-Calvente M, Calçada R, et al. Generalized probabilistic model allowing for various fatigue damage variables. Int J Fatigue 2017;100:187–94.
[60] Castillo E, Fernández-Canteli A, Hadi AS, López-Aenlle M. A fatigue model with local sensitivity analysis. Fatigue Fract Eng Mater Struct 2007;30(2):149–68.
[61] Ottosen NS, Ristinmaa M, Kouhia R. Enhanced multiaxial fatigue criterion that considers stress gradient effects. Int J Fatigue 2018;116:128–39.
[62] Ottosen NS, Stenström R, Ristinmaa M. Continuum approach to high-cycle fatigue modeling. Int J Fatigue 2008;30(6):996–1006.
[63] Carpinteri A, Fortese G, Ronchei C, Scorza D, Spagnoli A, Vantadori S. Fatigue life evaluation of metallic structures under multiaxial random loading. Int J Fatigue 2016;90:191–9.
[64] Pavlou DG. The theory of the s-n fatigue damage envelope: generalization of linear, double-linear, and non-linear fatigue damage models. Int J Fatigue 2018;110:204–14.
[65] Gao Z, Moan T. Fatigue damage induced by nonGaussian bimodal wave loading in mooring lines. Appl Ocean Res 2007;29(1):45–54.
[66] Benasciutti D, Tovo R. Fatigue life assessment in non-Gaussian random loadings. Int J Fatigue 2006;28(7):733–46.
[67] Portugal I, Olave M, Zurutuza A, López A, Muñiz-Calvente M, Fernández-Canteli A. Methodology to evaluate fatigue damage under multiaxial random loading. Eng Fract Mech 2017;185:114–23. xVIII International Colloquium Mechanical Fatigue of Metals.
[68] Aeran A, Siriwardane SC, Mikkelsen O, Langen I. A new nonlinear fatigue damage model based only on s-n curve parameters. Int J Fatigue 2017;103:327–41.
[69] Sun Q, Dui H-N, Fan X-L. A statistically consistent fatigue damage model based on miner's rule. Int J Fatigue 2014;69:16–21.
[70] Aid A, Amrouche A, Bouiadjra BB, Benguediab M, Mesmacque G. Fatigue life prediction under variable loading based on a new damage model. Mater Des 2011;32(1):183–91.
[71] Zuo F-J, Huang H-Z, Zhu S-P, Lv Z, Gao H. Fatigue life prediction under variable amplitude loading using a non-linear damage accumulation model. Int J Damage Mech 2015;24(5):767–84.
[72] Guo Q, Zaïri F, Guo X. An intrinsic dissipation model for high-cycle fatigue life prediction. Int J Mech Sci 2018;140:163–71.
[73] Xiao Y-C, Li S, Gao Z. A continuum damage mechanics model for high cycle fatigue. Int J Fatigue 1998;20(7):503–8.

[74] Cheng G, Plumtree A. A fatigue damage accumulation model based on continuum damage mechanics and ductility exhaustion. Int J Fatigue 1998;20(7):495–501.
[75] Oller S, Salomón O, Oñate E. A continuum mechanics model for mechanical fatigue analysis. Comput Mater Sci 2005;32(2):175–95.
[76] Dattoma V, Giancane S, Nobile R, Panella F. Fatigue life prediction under variable loading based on a new non-linear continuum damage mechanics model. Int J Fatigue 2006;28(2):89–95.
[77] Tang J, Hu W, Meng Q, Sun L, Zhan Z. A novel two-scale damage model for fatigue damage analysis of transition region between high- and low-cycle fatigue. Int J Fatigue 2017;105:208–18.
[78] Holopainen S, Kouhia R, Saksala T. Continuum approach for modelling transversely isotropic high-cycle fatigue. Eur J Mech A: Solids 2016;60:183–95.
[79] Zhang L, Song Liu X, Sen Wang L, Hui Wu S, Yuan Fang H. A model of continuum damage mechanics for high cycle fatigue of metallic materials. Trans Nonferrous Met Soc China 2012;22(11):2777–82.
[80] Shen F, Hu W, Meng Q, Zhang M. A new damage mechanics based approach to fatigue life prediction and its engineering application. Acta Mech Solida Sin 2015;28(5):510–20.
[81] Constantinescu A, Charkaluk E, Lederer G, Verger L. A computational approach to thermomechanical fatigue. Int J Fatigue 2004;26(8):805–18.
[82] Tateishi K, Hanji T, Minami K. A prediction model for extremely low cycle fatigue strength of structural steel. Int J Fatigue 2007;29(5):887–96.
[83] Rejovitzky E, Altus E. A micromechanical fatigue model with damage morphology. Int J Fatigue 2011;33(9):1235–43.
[84] Grandcoin J, Boukamel A, Lejeunes S. A micro-mechanically based continuum damage model for fatigue life prediction of filled rubbers. Int J Solids Struct 2014;51(6):1274–86.
[85] Eslami R, Riesch-Oppermann H, Kraft O. A micro-mechanical model for multiaxial high cycle fatigue at small scales. Procedia Eng 2014;74:57–63. xVII International Colloquium on Mechanical Fatigue of Metals (ICMFM17).
[86] Zhong B, Wang Y, Wei D, Wang J. A new life prediction model for multiaxial fatigue under proportional and non-proportional loading paths based on the pi-plane projection. Int J Fatigue 2017;102:241–51.
[87] Li B, Jiang C, Han X, Li Y. A new approach of fatigue life prediction for metallic materials under multiaxial loading. Int J Fatigue 2015;78:1–10.
[88] De-guang S, De-jun W. A new multiaxial fatigue damage model based on the critical plane approach. Int J Fatigue 1998;20(3):241–5.
[89] Li J, ping Zhang Z, Sun Q, wang Li C, jiang Qiao Y. A new multiaxial fatigue damage model for various metallic materials under the combination of tension and torsion loadings. Int J Fatigue 2009;31(4):776–81.
[90] Mei J, Dong P. A new path-dependent fatigue damage model for non-proportional multi-axial loading. Int J Fatigue 2016;90:210–21.
[91] Meggiolaro MA, de Castro JTP, Wu H. Computationally-efficient non-linear kinematic models to predict multiaxial stress-strain behavior under variable amplitude loading. Procedia Eng 2015;101:285–92. 3rd International Conference on Material and Component Performance under Variable Amplitude Loading, VAL 2015.
[92] Meggiolaro MA, de Castro JTP, Wu H. Non-linear incremental fatigue damage calculation for multiaxial non-proportional histories. Int J Fatigue 2017;100:502–11. multiaxial Fatigue 2016: Experiments and Modeling.
[93] yang Gao D, xing Yao W, Wu T. A damage model based on the critical plane to estimate fatigue life under multi-axial random loading. Int J Fatigue 2019.
[94] Correia J, Raposo P, Muniz-Calvente M, Blasón S, Lesiuk G, Jesus AD, et al. A generalization of the fatigue Kohout-Vechet model for several fatigue damage parameters. Eng Fract Mech 2017;185:284–300. xVIII International Colloquium Mechanical Fatigue of Metals.
[95] Benkabouche S, Guechichi H, Amrouche A, Benkhettab M. A modified nonlinear fatigue damage accumulation model under multiaxial variable amplitude loading. Int J Mech Sci 2015;100:180–94.
[96] Rege K, Pavlou DG. A one-parameter nonlinear fatigue damage accumulation model. Int J Fatigue 2017;98:234–46.
[97] Zhu S-P, Liao D, Liu Q, Correia JA, Jesus AMD. Nonlinear fatigue damage accumulation: isodamage curve-based model and life prediction aspects. Int J Fatigue 2019;128:105185.
[98] Kang HT, Lee Y-L, Chen J, Fan D. A thermo-mechanical fatigue damage model for variable temperature and loading amplitude conditions. Int J Fatigue 2007;29(9):1797–802. fatigue Damage of Structural Materials VI.
[99] Lu C, Melendez J, Martínez-Esnaola J. Fatigue damage prediction in multiaxial loading using a new energy-based parameter. Int J Fatigue 2017;104:99–111.
[100] Li Z, Ince A. A unified frequency domain fatigue damage modeling approach for random-on-random spectrum. Int J Fatigue 2019;124:123–37.
[101] Mamiya E, Castro F, Araújo J. Recent developments on multiaxial fatigue: the contribution of the university of brasília. Theoret Appl Fract Mech 2014;73:48–59 special Issue on Current models in multiaxial fatigue and fracture - in memory of Professor Ewald Macha.
[102] Wang Y-Y, Yao W-X. A multiaxial fatigue criterion for various metallic materials under proportional and nonproportional loading. Int J Fatigue 2006;28(4):401–8.
[103] Scott-Emuakpor O, George T, Cross C, Wertz J, Shen M-HH. A new distortion energy-based equivalent stress for multiaxial fatigue life prediction. Int J Non-Linear Mech 2012;47(3):29–37.
[104] Wang Z-L, Xiao H. Direct modeling of multi-axial fatigue failure for metals. Int J Solids Struct 2017;125:216–31.
[105] Djebli A, Aid A, Bendouba M, Amrouche A, Benguediab M, Benseddiq N. A non-linear energy model of fatigue damage accumulation and its verification for al-2024 aluminum alloy. Int J Non-Linear Mech 2013;51:145–51.
[106] Lee K-O, Hong S-G, Lee S-B. A new energy-based fatigue damage parameter in life prediction of high-temperature structural materials. Mater Sci Eng A 2008;496(1):471–7.
[107] Feng E, Wang X, Jiang C. A new multiaxial fatigue model for life prediction based on energy dissipation evaluation. Int J Fatigue 2019;122:1–8.
[108] Park J-B, Choung J, Kim K-S. A new fatigue prediction model for marine structures subject to wide band stress process. Ocean Eng 2014;76:144–51.
[109] de Lautour OR, Omenzetter P. Damage classification and estimation in experimental structures using time series analysis and pattern recognition. Mech Syst Signal Process 2010;24(5):1556–69 special Issue: Operational Modal Analysis.
[110] Pujol JCF, Pinto JMA. A neural network approach to fatigue life prediction. Int J Fatigue 2011;33(3):313–22.
[111] Durodola J, Ramachandra S, Gerguri S, Fellows N. Artificial neural network for random fatigue loading analysis including the effect of mean stress. Int J Fatigue 2018;111:321–32.
[112] Zhu J, Zhang W, Li X. Fatigue damage assessment of orthotropic steel deck using dynamic bayesian networks. Int J Fatigue 2019;118:44–53.
[113] Fathalla E, Tanaka Y, Maekawa K. Remaining fatigue life assessment of in-service road bridge decks based upon artificial neural networks. Eng Struct 2018;171:602–16.
[114] Franulovic M, Basan R, Prebil I. Genetic algorithm in material model parameters' identification for low-cycle fatigue. Comput Mater Sci 2009;45(2):505–10.
[115] Shabbir F, Omenzetter P. Model updating using genetic algorithms with sequential niche technique. Eng Struct 2016;120:166–82.
[116] Jimenez-Martinez M, Alfaro-Ponce M. Fatigue damage effect approach by artificial neural network. Int J Fatigue 2019;124:42–7.
[117] Kim H-J, Jang B-S, Park C-K, Bae YH. Fatigue analysis of floating wind turbine support structure applying modified stress transfer function by artificial neural network. Ocean Eng 2018;149:113–26.
[118] Müller K, Dazer M, Cheng PW. Damage assessment of floating offshore wind turbines using response surface modeling. Energy Procedia 2017;137:119–33. 14th Deep Sea Offshore Wind R&D Conference, EERA DeepWind'2017.
[119] Wong EWC, Kim DK. A simplified method to predict fatigue damage of ttr subjected to short-term viv using artificial neural network. Adv Eng Softw 2018;126:100–9.
[120] Lopes TAP, Ebecken NF. In-time fatigue monitoring using neural networks. Mar Struct 1997;10(5):363–87.
[121] Li CB, Choung J, Noh M-H. Wide-banded fatigue damage evaluation of catenary mooring lines using various artificial neural networks models. Mar Struct 2018;60:186–200.
[122] Bukkapatnam ST, Sadananda K. A genetic algorithm for unified approach-based predictive modeling of fatigue crack growth. Int J Fatigue 2005;27(10):1354–9. fatigue Damage of Structural Materials V.
[123] Low Y. A simple surrogate model for the rainflow fatigue damage arising from processes with bimodal spectra. Mar Struct 2014;38:72–88.
[124] Kim Y, Kim H, Ahn I-G. A study on the fatigue damage model for Gaussian wideband process of two peaks by an artificial neural network. Ocean Eng 2016;111:310–22.
[125] Jimenez M, Martinez J, Figueroa U. Load sequence analysis in fatigue life prediction. Trans Can Soc Mech Eng 2015;39(4):819–28.
[126] Hartt W, Lin N. A proposed stress history for fatigue testing applicable to offshore structures. Int J Fatigue 1986;8(2):91–3.